Type I interferons sensitise HIV-1-reactivating T-cells for NK cell-mediated elimination despite HDACi-imposed dysregulation of innate immunity

Julia Prigann[1,2,3], Dylan Postmus[1,2], Anna Julia Pietrobon[1,2], Emanuel Wyler[4], Jenny Jansen[1,2], Lars Möller[5], Jelizaveta Fadejeva[1,2], Thijs H. Steijaert[1,2], Cornelius Fischer[6], Uwe Koppe[7], Barbara Gunsenheimer-Bartmeyer[7], Karolin Meixenberger[8], Sarah N. Vitcetz[6], Madlen Sohn[6], Lucie Loyal[9], Andreas Thiel[9], Sascha Sauer[6], Kathrin Sutter[10], Ulf Dittmer[10], Michael Laue[4], Norbert Bannert[6], Markus Landthaler[3,11] and Christine Goffinet[1,2,12]

[1]Institute of Virology, Charité - Universitätsmedizin Berlin, Corporate Member of Freie Universität Berlin and Humboldt-Universität zu Berlin, Berlin, Germany

[2]Berlin Institute of Health (BIH), Berlin, Germany

[3]Gladstone Institute of Virology, San Francisco, CA 94158, USA

[4]Berlin Institute for Medical Systems Biology, Max Delbrück Center for Molecular Medicine in the Helmholtz Association, Berlin, Germany.

[5]Centre for Biological Threats and Special Pathogens, Robert Koch Institute, Berlin, Germany

[6]Scientific Genomics Platforms, Max Delbrück Center for Molecular Medicine in the Helmholtz Association, Berlin, Germany.

[7]Department of Infectious Disease Epidemiology, Robert Koch Institute, Berlin, Germany

[8]Sexually transmitted bacterial pathogens and HIV, Robert Koch Institute, Berlin, Germany.

[9]Si-M/"Der Simulierte Mensch" a Science Framework of Technische Universität Berlin and Charité – Universitätsmedizin Berlin, Berlin, Germany.

[10]Institute for Virology, University Hospital of Essen, Essen, Germany

[11]Institute for Biology, Humboldt-Universität zu Berlin, Berlin, Germany.

[12]Department of Tropical Disease Biology, Liverpool School of Tropical Medicine, Pembroke Place, Liverpool L3 5QA, U.K.

Christine Goffinet, Liverpool School of Tropical Medicine, Pembroke Place Liverpool, L3 5QA Liverpool, UK

29 Phone: +44(0)151 705 3100

30 e-mail: christine.goffinet@lstmed.ac.uk

31 **Keywords**: HIV-1 cure, shock-and-kill, single cell RNA-sequencing, HDACi, type I interferon

32

33 **ABSTRACT**

34 Shock-and-kill is one of the most advanced, yet unrealized, concepts towards establishment
35 of HIV-1 cure. Treatment with latency-reversing agents (LRAs), including histone deacetylase
36 inhibitors (HDACis) exerting chromatin remodelling and gene expression reprogramming,
37 combined with anti-retroviral therapy reactivates HIV-1 transcription *in vitro*, *ex vivo* and *in*
38 *vivo*. However, HDACi treatment fails to significantly reduce the size of the viral reservoir in
39 people living with HIV-1 (PLHIV). Here, by combining scRNA-seq and functional approaches,
40 we characterised the HDACi treatment-imposed remodulation of CD4+ T-cells' state and its
41 consequences for HIV-1 latency reversal and the apparent resistance of HIV-1-reactivating
42 cells to immune-mediated elimination. Exposure of $CD4^+$ T-cells from three aviremic PLHIV
43 with clinically applicable concentrations of Panobinostat markedly reduced the expression of
44 genes mediating T-cell activation and IFN-driven antiviral immunity in a largely $CD4^+$ T-cell
45 subset-nonspecific manner, with exception of an PLHIV-specific exhausted $CD4^+$ T-cell
46 subpopulation. Altered transcriptomic profiles were accompanied by large refractoriness to
47 peptide and IL-2/PHA stimulation, and to exogenous type I interferon, that would otherwise
48 induce T-cell activation and expression of a plethora of antiviral genes, respectively. Type I
49 interferon, when added to Panobinostat during HIV-1 reactivation, was unable to counteract
50 HDACi-mediated inhibition of IFN signalling and failed to interfere with HIV-1 reactivation *per*
51 *se*. However, it imposed a pre-budding block and boosted surface levels of HIV-1 Env on
52 reactivating cells. Co-treatment with type I IFNs, most prominently IFN-β and -α14, sensitised
53 HIV-1-reactivating cells for killing by NK cells through antibody-dependent cytotoxicity.
54 Together, our study provides proof-of-concept of the benefit of combining a potent LRA with
55 immunostimulatory molecules, such as type I IFNs, to reduce the resistance of HIV-1-

reactivating T-cells to immune-mediated elimination to improve current shock-and-kill strategies.

75 **INTRODUCTION**

76 Antiretroviral therapy (ART) effectively suppresses viremia and has improved the quality and
77 duration of life of people living with HIV/AIDS (PLHIV), but requires livelong adherence and is
78 not curative (1–4). HIV-1 persists as a viral reservoir in latently infected, long-lived CD4+ T-
79 cells with an estimated 73 years of optimal ART theoretically required for reservoir eradication
80 (5,6).

81 To accomplish ART-free remission, studies have focused on the reduction of the size
82 of the latent reservoir to achieve a functional HIV-1 cure (7). The shock-and-kill cure approach
83 is based on the administration of latency-reversing agents (LRAs) combined with ART with
84 the intention to reverse proviral quiescence in cellular reservoirs, an event that should be
85 followed by specific elimination of HIV-1-reactivating cells using immunological or
86 pharmacological mechanisms (8,9). Various classes of molecules, such as histone
87 deacetylase inhibitors (HDACis) (10–12), protein kinase C (PKC) agonists (13–15),
88 bromodomain and extraterminal domain (BET) protein inhibitors (16), second mitochondria-
89 derived activator of caspases (SMAC) mimetics (17), and Toll-like receptor (TLR) agonists
90 (18,19) have been explored for their ability to reverse HIV-1 latency *ex vivo* and *in vivo.* In
91 clinical trials individual LRAs demonstrate clear ability to reactivate HIV-1 transcription,
92 demonstrated by increased plasma viremia during continued ART. However, the size of the
93 viral reservoir in most studies decreased only to a minor extent, if at all (8,20) for poorly
94 understood reasons. One potential exception is the recent study in which treatment with
95 Venetoclax, a pro-apoptotic inhibitor of BCL-2, delayed viral rebound in a humanised mouse
96 model of HIV-1 infection, and depleted integrated HIV-1 DNA in $CD4^+$ T-cells from PLHIV (21),
97 suggesting that sensitising HIV-1-positive cells to apoptosis might enable reduction of the
98 reservoir size. Overall, existing data demonstrate an urgent need for a conceptual
99 improvement of the shock-and-kill approach.

100 Besides $CD8^+$ T-cell mediated mechanisms (22), NK cell-mediated antibody-
101 dependent cellular cytotoxicity (ADCC) has been proposed to contribute to natural, ART-free
102 control of HIV infection *in vivo*. Specifically, potent NK cells' anti-HIV activity was identified as

103 a discriminatory parameter in HIV-1 elite controllers as opposed to viremic progressors (23,24)
104 and as a specific characteristic of the few participants in the RV144 HIV-1 vaccine trial who
105 were protected from infection after immunisation (25,26). Type I IFNs increase the potency of
106 NK cells to eliminate HIV-1-infected cells *ex vivo* (27,28). Administration of pegylated IFN-
107 α2a or -α2b in combination with ART has resulted in sustained viral control in PLHIV and
108 declined levels of integrated HIV-1 DNA in the context of structured ART interruptions,
109 observations that associated with enhanced cytotoxic NK cell activity (29–35). Overall, there
110 is a growing body of evidence pointing towards a potential benefit of incorporating type I IFNs
111 into LRA-involving HIV-1 cure strategies, although the individual combinations of specific
112 LRAs with type I IFN have not yet been functionally tested in regards to both HIV-1
113 transcriptional reactivation and cell elimination.

114 Here, we characterise the transcriptional and functional profiles of $CD4^+$ T-cells from
115 PLHIV upon *ex vivo* exposure to two HDACis, Panobinostat and Vorinostat, to explore
116 potential cell-intrinsic properties contributing to the resistance of HIV-1-reactivating cells to
117 immune-mediated elimination *in vivo*. Using single-cell RNA sequencing we identified *ex vivo*
118 HDACi treatment to highly impact T-cell receptor and IFN-related innate immune signalling
119 pathways, resulting in a strong impairment of respective functions. Despite the extensive shut-
120 down of IFN signalling by Panobinostat treatment, type I IFN treatment, while not interfering
121 with HIV-1 reactivation *per se*, induced a block prior to viral budding. This phenotype was
122 accompanied by accumulation of viral Env on the surface of HIV-1-reactivating cells which
123 translated into a higher susceptibility to NK cell-mediated ADCC as compared to cells treated
124 with HDACi alone. In conclusion, this study provides proof-of-concept for combination of
125 potent LRAs with type I IFNs being a promising strategy to overcome the resistance of HIV-1-
126 reactivating T-cells to NK cell-mediated elimination. We propose that the results of our study
127 have important implications for improving current shock-and-kill strategies and will inform
128 future HIV-1 cure therapies.

129

130 **RESULTS**

131 **Panobinostat treatment modulates expression of CD4⁺ T-cell subset-specific markers**

132 In order to understand LRA-induced cellular phenotypes and CD4⁺ T-cell subpopulation-
133 specific susceptibilities to HDAC inhibition, we exposed purified CD4⁺ T-cells isolated from
134 three aviremic PLHIV (**Supplementary Table 1**) to Vorinostat, Panobinostat, IL-2/PHA or left
135 them mock-treated for 48 hours, followed by single cell RNA-sequencing. We selected
136 Vorinostat and Panobinostat as prototypic HDACis due to their demonstrated ability to
137 reactivate HIV-1 RNA expression *in vivo* (36,37). The applied concentrations of Vorinostat
138 (500 nM) and Panobinostat (50 nM) approached those detected in patients´ plasma after
139 single oral administration (11,36–38). We included IL-2/PHA treatment as a reference that we
140 expected to result in maximal activation of T-cells.

141 We used previously defined marker genes to identify the following T-cell subsets (39–
142 41): Naïve (T_N), central memory (T_{CM}), transitory memory (T_{TM}), effector memory (T_{EM}), effector
143 memory re-expressing CD45RA (T_{EMRA}) and regulatory (T_{REG}) T-cells in the dataset of mock-,
144 HDACi- and IL-2/PHA-treated CD4⁺ T-cells of PLHIV (**Fig. 1A**). In line with previous studies
145 (42), the T-cell subset distribution was not significantly altered in mock-treated samples from
146 aviremic PLHIV undergoing ART as compared to a culture from an HIV-1-negative donor (**Fig.**
147 **1B**). However, we confirmed the previously reported presence of a small subpopulation
148 specifically identified in cells from PLHIV (42,43), characterised by a combined and
149 significantly higher expression of the exhaustion markers *PDCD1*, *LAG3, HAVCR2, GZMB*
150 that was clearly separated from the otherwise similar T_{EMRA} cells (**Sup. Fig. 1**). Accordingly,
151 we referred to this subset as exhausted T-cells (T_{EX}).

152 Overall, Vorinostat-treated CD4⁺ T-cell cultures displayed very mild changes in subset
153 distribution as opposed to Panobinostat-treated culture that experience a complete loss of
154 cells expressing markers of T_{TM} (9.34% to 0%, $p = 0.0008$), T_{EMRA} (5.03% to 0%, $p = 0.0676$)
155 and T_{REG} (4.98% to 0%, $p = 0.0161$) subsets and a parallel increase in the proportion of T_{CM}
156 (23.9% to 35.57%, $p = 0.0155$). Relative levels of T_N (50.25% to 54.34%, $p = 0.0821$), T_{EX}

157 (0.43% to 1.11%, p = 0.778) and T_{EM} cells (6.06% to 5.18%, p = 0.2215) remained unchanged
158 under these experimental conditions (**Fig. 1B**). The observed changes in the T-cell subset
159 distribution induced by the individual treatments were detected in cell cultures from all three
160 donors to a similar extent (**Sup. Fig. 2**). Although we confirmed a low, but statistical significant
161 increase in both early and late apoptotic T-cells following Panobinostat treatment using a flow
162 cytometry-base viability assay, the complete loss of T_{TM}, T_{EMRA} and T_{REG} RNA marker-
163 expressing cells is unlikely to be explained by excessive, cell-type specific cell death (**Sup.**
164 **Fig. 3A-B**). Observed transcriptional changes correlated with reduced expression of multiple
165 T-cell marker on the cell surface following Panobinostat, but not Vorinostat, treatment,
166 including CD3, CD4, CD45RA (marker for naïve T-cells), CD62L (SELL), CD45RO (marker
167 for memory T-cells), HLA-DR (late marker for activated T-cells), CXCR4, and most
168 pronounced, the cytokine receptor IL7R/CD127 (**Sup. Fig. 3C**). CCR5 and CD69 cell surface
169 expression were mildly increased in the context of Panobinostat treatment, corroborating
170 previous reports of transient CD69 expression following Panobinostat treatment from *in vivo*
171 (44) and *ex vivo* (38) studies (**Sup. Fig. 3D**). Together, among the two HDACi treatments
172 conducted under indicated experimental conditions, Panobinostat induced a massive
173 rearrangement of $CD4^+$ T-cell subset marker expression, both on the transcriptional and
174 translational level.

175 **Panobinostat treatment induces broad transcriptional down-modulation of genes**
176 **involved in T-cell signalling and a subset of genes implicated in innate immunity**

177 Vorinostat treatment induced modest gene expression changes, with expression of 1.388
178 genes induced and 312 genes decreased (**Fig. 2A**). In contrast, Panobinostat treatment
179 altered the expression of a total of 10.119 genes. Comparing the two HDACi treatments, 4.078
180 genes were up-regulated and 5.124 were down-regulated in Panobinostat- compared to
181 Vorinostat-treated cells. Focussing on genes with >2-fold change in expression, cultures
182 treated with individual HDACis displayed a substantial overlap of DEGs, suggesting that
183 transcriptomic alterations were partially similar (**Fig. 2B**). Gene sets previously associated with

184 Notch signalling, synaptic vesicle trafficking and Alzheimer's disease-presenilin were enriched
185 in Panobinostat-treated cell cultures (**Fig. 2C**). Pathways that were downregulated in the
186 context of Panobinostat treatment were associated with T-cell activation, cytokine- and
187 chemokine-mediated inflammation and JAK/STAT signalling (**Fig. 2C**), in line with reduced
188 activity of multiple transcription factors in all T-cell subsets essential for mediating innate and
189 T-cell-specific immune responses, such as IRF9, STAT1, STAT2, NFKB1 and STAT5,
190 GATA3, RELA, respectively (**Fig. 2D**). Interestingly, activity scores of IRF3 and STAT6 were
191 increased in T_N- and T_{CM}-cell subsets (**Fig. 2D**), suggesting partial, subset-specific activation
192 of innate signalling cascades. Vorinostat failed to enrich or deplete specific gene sets,
193 corroborating the minor impact of Vorinostat at the applied concentration on the overall T-cell
194 transcriptomic profile.

195 Base-line expression of IFN-stimulated genes (ISGs) in untreated cells was to a certain
196 extent subset-specific (**Fig. 2E**). For example, *LGALS3BP* and *IFI44L* displayed the highest
197 expression in resting T_N- and T_{CM}-cell subsets, respectively, while *OASL* and *APOBEC3G*
198 expression was highest in T_{EM}- and T_{EMRA}-cells. The observations on the individual ISG
199 expression level were corroborated by the IFN Module Score that takes expression of multiple
200 genes associated with IFN signalling into account. T_N-, T_{CM}- and T_{TM}-cells displayed an overall
201 modest, T_{EM}-, T_{EMRA}- and T_{REG}-cells gradually increasing and T_{EX}-cells a relatively low IFN
202 Module Score in mock-treated $CD4^+$ T-cells (**Fig. 2F**). Overall, Vorinostat treatment only mildly
203 affected the ISG expression pattern and IFN Module Score (**Fig. 2E-F**). In contrast,
204 Panobinostat-exposed $CD4^+$ T-cells displayed drastically decreased levels of the majority of
205 ISGs, including *ISG20*, *MX1*, *IFI44L*, *IFITM1*, *XAF1*, *GBP2*, *IFI16* throughout all subsets and
206 reduced expression of *IFI27*, *IFITM3*, *IFIT3*, *IFIT2* and *BST2* in T_N-, T_{CM}- and T_{EM}-cells, with
207 an opposite trend in T_{EX}-cells (**Fig. 2E**). However, *IFIT1, STAT1, IFI30 and RASD2* expression
208 was increased after Panobinostat treatment in all subsets, with *IFIT1* and *STAT1* expression
209 found to be most pronounced in T_{EX}-cells, and *IFI30* and *RASD2* expression to be particularly
210 induced in T_{EM}-cells (**Fig. 2E**). Interestingly, we previously reported expression of these four
211 genes specifically to be upregulated in the context of base-line cGAS activity (45), which drives

212 IRF3-controlled gene expression, suggesting a partial and CD4$^+$ T-cell subset-specific
213 activation of IRF3 following Panobinostat treatment. Nevertheless, the overall IFN Module
214 Score taking the average expression of hundreds of ISGs into account was decreased in all
215 Panobinostat-treated T-cell subsets, while it was largely maintained upon Vorinostat treatment
216 (**Fig. 2F**).

217 We established a drastic down-regulation of genes involved in T-cell signalling and
218 activity following Panobinostat, but not Vorinostat treatment (**Fig. 2G-H**). As expected under
219 mock treatment conditions, expression of genes whose products regulate and mediate T-cell
220 signalling and activation was clearly T-cell subset-specific (**Fig. 2G-H**). Panobinostat
221 treatment induced downregulation of expression of multiple T-cell function-specific genes,
222 including *IL4R*, *LAT*, *IL6R*, *ZAP70*, and those for which we had detected reduced protein
223 expression on cell surface (CD62L (*SELL*), HLA-DRA, CD45RA/CD45RO (*PTPRC*), IL7R,
224 CCR5 and CD3 (*CD3G*)). Some T-cell-specific genes were specifically upregulated in T_{EX}-
225 cells, including *CD4*, *MAP3K1*, *CSK* and *AKT3*. In accordance with the transient nature of
226 CD69 expression upon Panobinostat treatment (**Sup. Fig. 3D**), *CD69* mRNA expression at 48
227 hours equaled those of mock-treated cells. The overall trend of reduced T-cell activation-
228 specific gene expression was reflected in a T-cell Activation Module Score of Panobinostat-
229 treated cells that was reduced to below the average of mock- and Vorinostat-treated cells (**Fig.
230 2H**).

231 In order to test to which extent HDACi-imposed gene expression changes can be
232 recapitulated in a more amenable HIV-1 latency cell system, we treated J1.1 T-cells, that
233 harbour at least two replication-competent HIV-1 proviruses per cell (46,47) with Vorinostat
234 and Panobinostat (**Sup. Fig. 4**). Here, we applied concentrations of HDACis (16 µM Vorinostat
235 and 200 nM Panobinostat) that induced a similar degree of HIV-1 reactivation as judged by
236 intracellular HIV-1 p24 expression (**Sup. Fig. 4A**). Both treatments resulted in a similar number
237 of down- and upregulated genes (**Sup. Fig. 4B**) with a substantial overlap of modulated genes
238 (**Sup. Fig. 4C**). The concentration of applied Panobinostat in J1.1 T-cells (200 nM)
239 approached the one used in primary CD4$^+$ T-cells (50 nM) and induced partially similar gene

240 expression changes. Specifically, downregulated activity scores of transcription factors
241 required for T-cell signalling (**Sup. Fig. 4D**), in line with reduced expression of genes related
242 to T-cell activity, such as *CD3G*, *SELL*, *LAT*, *STAT5A* or *ZAP70* and a significantly reduced
243 T-cell Activation Module Score (**Sup. Fig. 4E**). The ISG expression profile following
244 Panobinostat was less well conserved between J1.1 T-cells and CD4+ T-cells. While
245 Panobinostat-treated primary $CD4^+$ and J1.1 T-cells shared expression profiles of some ISGs
246 (downregulation of *MX1*, *MX*2, *OAS1*, *XAF1*, *BST2*; upregulation of *GBP5*, *STAT1*, *IFIT1*),
247 they differed regarding expression of *LGALS3BP*, *GBP2*, *IFI44L*, *OASL* (**Sup. Fig. 4F**),
248 resulting in an overall elevated IFN Module Score in J1.1 T-cells as opposed to primary $CD4^+$
249 T-cells.

250 Conclusively, under these experimental conditions, Panobinostat, and, if applied at
251 higher concentration, also Vorinostat, significantly reduced expression of several genes that
252 are essential for T-cell-specific immune responses and a part of IFN-modulated genes.

253

254 **HDAC inhibition imposes a block to $CD4^+$ T-cell activation and type I IFN signalling**

255 We hypothesised that HDACi-induced modulation of gene expression is of functional
256 relevance for HIV-1 reactivation and immune recognition of reactivating cells. To investigate
257 the result of HDACi treatment on T-cell activation, we pre-incubated $CD4^+$ T-cells from HIV-1-
258 negative donors with HDACis prior to inducing T-cell activation by IL-2/PHA (**Fig. 3A**). Pre-
259 incubation with DMSO or Vorinostat resulted in marked IL-2/PHA-triggered enhancement of
260 the percentage of cells expressing the activation markers CD69, CD25, HLA-DR and also the
261 exhaustion markers TIM-3 and PD-1, indicating successful T-cell activation. Conversely,
262 Panobinostat pretreatment resulted in impaired induction of CD69 expression (0.49-fold
263 changed), and in a complete lack of IL-2/PHA-mediated induction of expression of CD25, HLA-
264 DR, TIM-3 and PD-1 (**Fig. 3A**). To study TCR-induced T-cell activation, we preincubated $CD4^+$
265 T-cells with HDACi followed by treatment with a universal peptide pool in combination with an
266 anti-CD28 antibody. Expression of the early activation marker CD69 after TCR stimulation was
267 slightly, but statistically significantly induced in Vorinostat- (1.65-fold) and to a higher extent in

268 Panobinostat-pretreated samples (5.5-fold), suggesting efficient initiation of T-cell activation
269 in the presence of both HDACis (**Fig. 3B**). Expression of the middle activation marker CD25,
270 the exhaustion marker PD-1 and the late activation marker HLA-DRA increased upon TCR
271 stimulation in the context of Vorinostat pretreatment (2.07-, 2.07- and 1.39-fold change,
272 respectively), suggesting that weak HDAC inhibition does not prevent TCR-specific T-cell
273 activation. However, expression of CD25 and HLA-DRA was severely reduced in
274 Panobinostat-pretreated cultures (0.05- and 0.47-fold change, respectively), suggestive of
275 abortive peptide-induced T-cell activation.

276 We next examined the impact of HDAC inhibition on type I IFN signalling and ISG
277 expression. Specifically, we treated $CD4^+$ T-cells isolated from HIV-1-negative donors with
278 DMSO, Vorinostat or Panobinostat in combination with increasing concentrations of IFN-α2a
279 and assessed cell surface expression changes of BST-2 and changes of *IFIT1* and *MX2* gene
280 expression (**Fig. 3C-D**). We applied an increased concentration of Vorinostat in these
281 experiments to adjust for the inferior potency of Vorinostat compared to Panobinostat that has
282 been reported in previous studies (38,48). Both Vorinostat and Panobinostat significantly
283 dampened base-line BST-2 cell surface expression levels, and both tested concentrations
284 (100 and 1000 IU/ml) of IFN-α2a failed to rescue the HDACi-imposed block to BST2 surface
285 expression (**Fig. 3C**). Interestingly, mRNA expression levels of the two ISGs *IFIT1* and *MX2*
286 showed a divergent phenotype. Individual treatment with Vorinostat and Panobinostat, as well
287 as addition of IFN-α2a, induced and further amplified *IFIT1* mRNA expression, respectively
288 (**Fig. 3D**). In contrast, *MX2* mRNA expression decreased in the context of HDACi treatment,
289 both in the absence and presence of 1000 IU/ml IFN-α2a (**Fig. 3E**). These results were
290 paralleled in latently HIV-1-infected J1.1 T-cells in which HDAC inhibition, but not treatment
291 with the non-HDACi LRA Bryostatin, reverted prior IFN-α2a-induced expression of MX2 in a
292 dose-dependent manner and abolished the negative impact of IFN on early HIV-1 reactivation
293 as judged by intracellular p24 expression (**Sup. Fig. 5A).** Co-administration of increasing
294 doses of IFN-α2a up to 10,000 IU/ml was insufficient to counteract the HDACi-suppressed
295 MX2 expression and did not limit the efficiency of HIV-1 reactivation, in contrast in the context

296 of Bryostatin treatment, IFN treatment induced MX2 expression efficiently and inhibited HIV-1
297 reactivation in a dose-dependent fashion (**Sup. Fig. 5B**).
298 Together, HDAC inhibition renders CD4$^+$ T-cells largely refractory, and/or less
299 sensitive, to mitogen and TCR stimulation and dampens the base-line and IFN-induced
300 expression of multiple ISGs, including the two prototypic ISGs BST-2 and MX2, while IRF3-
301 driven expression of a small subset of ISGs remains intact and is even exacerbated. We
302 hypothesise that the HDACi-induced cellular phenotypes both at the level of CD4$^+$ T-cells as
303 HIV-1 reactivating target cells, and CD4$^+$ T-cell effector functions is likely to contribute to the
304 lack of HIV-1-positive T-cell elimination *in vivo* both at the level of CD4$^+$ T-cells as HIV-1
305 reactivating target cells, and CD4$^+$ T-cell effector functions.
306
307 **Addition of IFN-α2a to Panobinostat results in a tetherin-independent pre-budding**
308 **defect**
309 The previous data highlighted that HDAC inhibition significantly diminishes IFN-induced
310 signalling, potentially nullifying the negative effect of IFN on HIV-1 replication. To test in detail
311 the impact of IFN on HIV-1 reactivation and multi-round spread upon LRA treatment, J.1. T-
312 cells were primed with a single dose of 50 nM Panobinostat in the presence or absence of
313 IFN-α2a. The percentage of HIV-1 p24 capsid-expressing cells was initially similar, but differed
314 starting from day three on (**Fig. 4A**, **Sup. Fig. 6**). Addition of IFN to Panobinostat reduced the
315 abundance of p24 capsid (**Fig. 4B**) and infectivity (**Fig. 4C**) released into cell culture
316 supernatant, effects detectable from day two and one post-treatment start on, respectively.
317 Two days post HIV-1 reactivation, a time point at which cell-associated p24 capsid expression
318 is statistically indistinguishable (**Fig. 4A**), the morphology of budding sites was similar and
319 intact in both conditions (**Fig. 4D**), however, the incidence of detectable budding events per
320 cell was reduced 2.2-fold in the context of the co-treatment (**Fig. 4E**). Importantly, this
321 observation was obtained in the absence of tetherin-imposed attachment of virions to the cell
322 surface or to each other (**Fig. 4D)**. This tetherin-atypical microscopic appearance, and the lack
323 of IFN-induced tetherin upregulation when Panobinostat is present (**Fig. 4F, G**) strongly

324 argues against tetherin driving this antiviral phenotype, and rather suggests a defect prior to
325 release or a tetherin-independent release defect.
326
327 **IFN-induced virus pre-budding block is accompanied by accumulation of HIV-1 Env on**
328 **cellular and viral membranes**
329 Next, we assessed the nature of the IFN-imposed block prior to HIV-1 budding. Despite
330 increasing concentrations of IFN-α2a, Panobinostat-induced cell-associated HIV-1 p24 capsid
331 expression remained intact (**Fig. 5A**). In contrast, the p24 capsid signal intensity in
332 corresponding supernatants (**Fig. 5B**) and normalised release (**Fig. 5C**) dose-dependently
333 decreased in cultures co-treated with IFN-α2a. Interestingly, combined Panobinostat/IFN-α2a
334 treatment resulted in a higher ratio of gp120 per p24 (**Fig. 5D**), suggesting a higher rate of
335 Env incorporation in released virions in the absence of evidence for an Env processing
336 alteration in corresponding cell lysates (**Sup. Fig. 7A**). Panobinostat, alone or in combination
337 with IFN-α2a, increased the percentage of cells expressing HIV-1 Env on their surface (**Fig.**
338 **5E**), in line with increase of cell-associated p24 expression by both conditions (**Fig. 5A**).
339 However, IFN-α2a addition to Panobinostat had a 1.32-fold, statistically significant increase of
340 the mean fluorescence intensity (MFI) of Env signal on Env-positive cells as a consequence,
341 indicating accumulation of HIV-1 Env molecules on the cell surface (**Fig. 2F**). Treatment with
342 the JAK/STAT inhibitor Ruxolitinib preserved the increase of percentage of Env-positive cells
343 (**Sup. Fig. 7B**), but nullified IFN-induced Env accumulation per cell (**Sup. Fig. 7C**), consistent
344 with upregulation of Env requiring functional IFN signalling. Conclusively, combined treatment
345 of Panobinostat and IFN-α2a results in increased quantities of HIV-1 Env on reactivating T-
346 cells´ surfaces and released virions.
347
348 **Addition of IFN-α2a to Panobinostat enhances the susceptibility of reactivating T-cells**
349 **to NK-mediated antibody-dependent cellular cytotoxicity**
350 Being the sole viral antigen presented on the virus-producing cell surface, HIV-1 Env protein
351 serves as the major target of antibody-mediated responses. We therefore examined whether

352 the increased surface expression of HIV-1 Env in the context of IFN-α2a treatment renders
353 cells more susceptible to ADCC. Specifically, we co-cultured HIV-1-reactivating, cell tracker™
354 Green-CMFDA-stained J1.1 T-cells and freshly isolated PBMCs in the presence of serum from
355 PLHIV, and loss of HIV-1 p24 capsid-positive cells was monitored (**Sup. Fig. 8A**). ADCC
356 decreased with increasing dilutions of the anti HIV-1-Env antibody-containing serum,
357 independent of the reactivation regimen applied (**Fig. 6A-C**). Interestingly, Panobinostat
358 treatment failed to significantly enhance ADCC as compared to DMSO treatment, suggesting
359 that it increases the quantities of HIV-1 p24- and Env-positive cells, but not their relative
360 susceptibility to antibody-mediated elimination. In contrast, J1.1 T-cells reactivated in the
361 presence of IFN-α2a scored overall higher ADCC values. T-cells co-cultured with isolated NK
362 cells, but not monocytes, displayed a statistically significant increase of ADCC in the context
363 of IFN-α2a co-treatment as compared to Panobinostat only-treatment (**Sup. Fig. 9A, B**),
364 arguing for a predominant role of NK cells rather than monocytes in mediating T-cell killing. In
365 line with this, CD107a surface exposure and CD16 downregulation, which strongly correlates
366 with NK cell activation, cytokine production and target cell lysis (47–49), were highly induced
367 in the NK cell population of PBMCs co-cultured with J1.1 T-cells (**Sup. Fig. 9C-E**). Co-
368 treatment of J1.1 T-cells with Panobinostat and IFN-α2a, however, did not result in notable
369 differences of the two Panobinostat-treated conditions in regards to NK cell effector activation
370 despite increased target cell killing in the co-culture (**Sup. Fig. 9D-E**), arguing for IFN-a2
371 increasing the sensitivity of target cells to killing rather than modulating effector cell activity.

372 We next investigated whether IFN-α2a addition modulates the kinetics of NK cell-
373 effected ADCC against Panobinostat-treated J1.1 T-cells using live-cell imaging. Specifically,
374 J1.1 T-cells were treated either with Panobinostat only or Panobinostat in combination with
375 IFN-α2a for 48 hours, followed by differential staining of these two J1.1 T-cell cultures using
376 Cell Tracker™ Green CMFDA and Cell Tracker™ Deep Red, respectively. Cells were then co-
377 cultured with freshly isolated, unstained NK cells at a 1:1:1 ratio in the presence of serum from
378 PLHIV and a cell death marker (blue) and imaged every three minutes for a total of four hours
379 (**Sup. Movie 1**). The starting frame contained similar numbers of both J1.1 T-cell cultures (47

380 green cells, 51 red cells). As expected, the overall number of cell death marker-positive J1.1
381 T-cells increased over time, indicating ADCC. We did not detect profound differences
382 regarding the duration of individual NK cell/J1.1 T-cell interactions depending on the T-cell line
383 pretreatment (**Sup. Movie 1**). However, the percentage of cells dying until the end of the
384 experiment, as judged by acquisition of the blue fluorescence and visual disappearance was
385 clearly increased for cells receiving Panobinostat/IFN-α2a co-treatment (31.4%) as compared
386 to cells pre-treated with Panobinostat alone (12.8%) (**Fig. 6E**). The number of
387 Panobinostat/IFN-α2a-treated J1.1 T-cells showing signs of cell death increased rapidly and
388 plateaued at 69 minutes after the start of the imaging (**Fig. 6F**). In contrast, the number of
389 Panobinostat-treated J1.1 T-cells with signs of cell death increased only moderately and
390 plateaued after 75 minutes (**Fig. 6F**). Despite the high mobility and intact shape of the NK
391 cells, no more J1.1 T-cells were eliminated 75 minutes after start of the co-culture, suggesting
392 that the remaining J1.1 T-cells either did not reactivate HIV-1 expression or were otherwise
393 resistant to killing. Of note, a substantial fraction of NK cells that otherwise presented an intact
394 cell shape and high mobility acquired the blue death marker over time (**Sup. Movie 1**). We
395 hypothesise that the processes of degranulation and re-internalization of granules in highly
396 active NK cells allow the uptake of the cell death dye from the medium, not necessarily
397 reflecting cell death. This is in line with the observation that specifically the highly mobile, J1.1
398 T-cell-interacting NK cells stained positive for the cell death marker, the same population of
399 cells that is thought to have a high cytotoxic potential.
400 Overall, our observations are in line with a scenario in which addition of IFN-α2a to a
401 Panobinostat-mediated HIV-1 reactivation regimen renders HIV-1-positive cells more prone to
402 NK cell-mediated ADCC, in line with higher levels of the major antibody target Env on the cells'
403 surface, despite similar levels of HIV-1 reactivation.
404

405 **IFN-α2a-enhanced HIV-1 Env cell surface accumulation and ADCC sensitization occur**
406 **in the context of HDACi-, but not PKC agonist-mediated HIV-1 reactivation**

407 We next tested whether IFN-α2a-mediated upregulation of HIV-1 Env and sensitivity of cells
408 to immunological elimination occurs in conjunction with a specific class of LRA or, on the
409 contrary, universally upon HIV-1 latency reversal. Like Panobinostat treatment, individual
410 treatment of cells with the HDACis Vorinostat and Romidepsin, and the PKC agonist Bryostatin
411 strongly increased the percentage of HIV-1 p24 capsid-positive cells, while the BET inhibitor
412 JQ1 was inferior in reversing proviral quiescence (**Sup. Fig. 10A**). Overall, the percentages of
413 HIV-1 Env-positive cells induced by Vorinostat, Romidepsin and JQ1 treatment followed the
414 percentages of p24-positive cells. Surprisingly Bryostatin treatment, both in the absence or
415 presence of IFN-α2a, failed to increase the percentage of Env-positive cells, despite clear HIV-
416 1 reactivation at the level of p24 capsid (**Sup Fig. 10B**), and accordingly, both treatments did
417 not alter susceptibility to ADCC which, surprisingly, was clearly detectable despite low surface
418 Env levels (**Sup. Fig. 10C**). In summary, our findings suggests that IFN-α2a co-treatment
419 enhances Env cell surface expression in the context of HDACi and the iBET JQ1, but not
420 Bryostatin, pointing towards LRA class-specific differences in HIV-1 Env cell surface targeting
421 and/or regulation.
422

423 **The ability to restrict HIV-1 budding and facilitate elimination of HIV-1-positive T-cells**
424 **is type I IFN protein-specific**

425 Although previous HIV-1 cure strategies focused on incorporation of IFN-α2a or -α2b in shock-
426 and-kill approaches, *in vitro* work clearly demonstrates that other members of the type I IFN
427 family, including IFN-α6, IFN-α14 and IFN-β, display superior anti-HIV-1 properties (49–52).
428 To investigate the breadth of type I IFN proteins to enhance susceptibility of HIV-1-reactivating
429 cells to elimination, we selected IFN-α6, IFN-α14 and IFN-β due to their previously reported
430 high anti-HIV-1 activity (49,50,52), IFN-α16 for its comparatively weaker activity (49,50,52)
431 and IFN-α2 as a reference. IFN-α14 and -β treatment resulted in strongest ISG induction, as
432 judged by quantification of *IFIT1* mRNA and BST-2 protein expression (**Sup. Fig. 11**). Upon
433 co-treatment with Panobinostat, all tested type I IFNs, particularly IFN-α14 and -β, significantly
434 decreased secreted infectivity (**Fig. 7A**). Surprisingly, all IFNs shared the ability to increase

435 the HIV-1 Env surface MFI (**Fig. 7B**), but differed in their ability to sensitise T-cells for
436 elimination, with IFN-α14 and -β treatment resulting in highest ADCC rates (**Fig. 7C**). It is
437 worth mentioning that the activity of the in-house generated IFN subtypes used in Fig. 7 was
438 determined using an ISRE-reporter cell line in contrast to commercial IFN-α2a (Roferon, used
439 in the rest of the study) whose activity is quantified in a cytopathic effect inhibition assay.
440 These differences hindered a direct comparison of the two IFN-α2 potencies and potentially
441 explain the relative lack of IFN-α2 in inducing ADCC under these experimental conditions (**Fig.
442 7C**). The antiviral activity of individual type I IFN proteins correlated with the induced
443 susceptibility to ADCC. The degree of upregulation of cell surface Env levels did not predict
444 ADCC susceptibility (**Fig. 7D**), suggesting that IFN-mediated enhancement of surface Env
445 levels is required, but not sufficient for sensitising cells to elimination.

446 In summary, we identified a superior ability of the clinically yet underexplored members
447 of the type I IFN family, IFN-α14 and -β, to enhance susceptibility to elimination of HIV-1-
448 reactivating T-cells which correlates with their ability to inhibit HIV-1 budding in the context of
449 Panobinostat reactivation and to accumulate viral Env on the HIV-1-reactivating cells' surface.
450

451 **DISCUSSION**

452 The overarching aim of LRA treatment in the context of HIV-1 cure is reinitiation of HIV-1
453 mRNA and protein expression to a degree that is sufficient to render a maximum of HIV-1-
454 reactivating cells immunologically visible, making them susceptible to elimination. The ability
455 of HDACis to reverse HIV-1 latency *in vitro* and *in vivo* (12,36–38,53) involves hyperacetylation
456 of histones, which leads to opening of cellular chromatin and subsequently modulation of
457 gene expression, including transcriptional reactivation from dormant HIV-1 genomes (54,55).
458 LRA treatment *per se* influences the expression profile of a plethora of cellular genes, with to
459 date poorly defined consequences on cellular processes affecting HIV-1 RNA stability, HIV-1
460 protein expression, trafficking and cell surface presentation, and finally susceptibility of HIV-
461 1-reactivating cells to cytotoxicity. An optimal shock-and-kill regimen should, on the one hand,
462 mount a proviral milieu that facilitates post-integration steps of the virus replication cycle. On

463 the other hand, in a second step, an ideal shock-and-kill regimen must render reactivating T-
464 cells susceptible to recognition and killing by CD8$^+$ T-cell and NK cell-mediated cytotoxicity,
465 processes that are orchestrated in the effector cell, among others, by functional type I IFN
466 signalling (27,56). Treatment of CD4$^+$ T-cells with Panobinostat resulted in a markedly
467 impaired ability to respond to activation stimuli, including TCR/CD28 and IL-2/PHA, in line with
468 reports of HDACi treatment-induced antigen-specific anergy of mouse lymphocytes (57).
469 Given that Panobinostat treatment compromises functionality of NK cells (58) and CD8$^+$ T-
470 cells (59,60), it is tempting to speculate that it also affects the efficiency of peptide processing
471 and presentation in HIV-1-reactivating CD4$^+$ T-cells by MHC-I molecules. Along this line,
472 HDACi treatment has been proposed to reduce cytosolic peptidase activities in *ex vivo*-HIV-
473 1-infected CD4$^+$ T-cells, resulting in modulated antigen presentation to CD8$^+$ T-cells (61).
474 Together, we suspect that these effects compromise the overall effector functions of several
475 immune cell types that would otherwise contribute to elimination of HIV-1-reactivating T-cells.
476 A second striking consequence of Panobinostat was a largely CD4$^+$ T-cell subset
477 unspecific, broad, though not entire shut-down of components of IFN-related signalling
478 pathways and functions, which is consistent with the known requirement of functional histone
479 deacetylation for IFN signalling, but not for IRF3-mediated gene expression programmes (62).
480 This leads us to propose to re-consider the contribution of several antiviral genes when
481 analysed in the context of HDACi-induced reactivation, since expression of several ISGs is
482 repressed by HDACi treatment even in the presence of high concentrations of type I IFN. A
483 striking example is our observation of an IFN-induced release defect. Iin the context of
484 Panobinostat treatment, tetherin expression is downregulated in most CD4$^+$ T-cell
485 subpopulations except the exhausted CD4+ T-cell subset, fully prevented even when type I
486 IFN is exogenously added, and the microscopic appearance of stalled budding events
487 resembles more those described in the context of ESCRT component defects (63). Together,
488 these data argue rather for a to date unknown ISG product whose IFN dependency is still
489 preserved despite HDAC inhibition.

490 Type I IFN treatment in conjunction with Panobinostat-mediated HIV-1 reactivation
491 was followed by increase of HIV-1 Env molecule density on viral and HIV-1-reactivating T-
492 cells' surfaces. HIV-1 tightly regulates the presentation of Env on the cell surface to minimise
493 the vulnerability against humoral responses while maintaining infectivity (64). The observed
494 Env cell surface accumulation may be an indirect consequence of the pre-budding defect,
495 where fewer virions are detached from the producer cell, resulting in excess HIV-1 Env at the
496 plasma membrane, and/or may be a direct consequence of the HDACi/IFN treatment
497 combination on HIV-1 Env trafficking and recycling. The rate of internalisation of Env
498 molecules and their conformation presented at the cell surface have been reported as
499 determinants of the HIV-1-infected cell's susceptibility to ADCC (65–67). Our data points
500 towards a scenario in which, in the context of Panobinostat treatment, increased Env
501 expression on reactivating T-cells, likely with contribution of a potential ISG product, sensitises
502 HIV-1-reactivating T-cells for NK cell-mediated elimination. This would represent a novel
503 mechanism by which type I IFN sensitises, rather than protects, target cells for elimination. On
504 the contrary, several studies reported type I IFNs to protect T-cells from NK cell-mediated
505 cytotoxicity by processes involving upregulation of expression of selected inhibitory NK-cell-
506 receptor ligands (68) and reduction of expression of natural cytotoxicity triggering receptor 1
507 (NCR1) ligands as evasion mechanism (69). However, these studies were not conducted in
508 the context of pharmacological reactivation of HIV-1. Specifically, a higher proportion of
509 Panobinostat-only treated cells remained viable at the end of the co-culture as compared to
510 IFN-co-treated cells, indicating an intrinsic resistance to ADCC-mediated killing that was
511 partially overcome by the addition of IFN. Importantly, we did not observe differences in the
512 degranulation activity or cellular activation of NK cells retrieved from co-cultures with either
513 Panobinostat- or Panobinostat/IFN-treated J1.1 cells, suggesting that the impact of IFN on NK
514 cell effector activity is neglectable under these experimental conditions. To date, only tetherin
515 has been identified as an IFN-stimulated factor that augments ADCC responses against HIV-
516 1-infected cells (67,70) however, it is an unlikely candidate in the context of Panobinostat
517 treatment due to its virtually absent expression in the context of HDAC inhibition. Adding

518 another layer of complexity, susceptibility to immune-mediated clearance is not determined be
519 mere quantities of surface-accessible Env, as evidenced by our data showing clear antibody-
520 dependent killing despite low cell surface levels of Env on target T-cells following Bryostatin-
521 mediated latency reversal, and IFN-protein-specific ADCC susceptibilities despite similar Env
522 cell surface levels following Panobinostat treatment. The characterisation of cellular and viral
523 factors that determine the susceptibility of HIV-1-reactivating cells to ADCC and how these
524 factors are manipulated by individual pharmacologic latency reversal strategies are key
525 questions to be addressed in future studies.

526 In the context of HIV-1 shock-and-kill cure approaches, HDACis belong to the most
527 thoroughly studied class of LRAs and are well tolerated *in vivo* (71,72), though administration
528 of HDACis appears to inhibit essential immune effector functions of $CD8^+$ T-cells (60), NK cells
529 (58,73) and reduce susceptibility of target T-cells to cytotoxic elimination as shown in our
530 study. However, the overall high potency of HDACis to reactivate HIV-1 and the lack of
531 alternative LRAs with better *in vivo* performance encourages the continued use of HDACis in
532 newly launched clinical trials, especially in combination with immunomodulatory drugs to
533 counterbalance the HDACi-mediated negative effects. Currently, HDACis are being tested in
534 combination with pegylated IFN-α2a (Clinical trial NCT02471430), broadly neutralising
535 antibodies (Clinical trial NCT02850016) (74,75) and therapeutic vaccine candidates (Clinical
536 trials NCT02092116 and NCT02616874) (76). Within this conceptually broad field, our study
537 is the first proof-of-concept that provides a mechanistic rationale that justifies incorporating
538 type I IFNs in shock-and-kill settings to enhance the susceptibility of HIV-1-reactivating T-cells
539 to immune-mediated elimination. Importantly, the superior ability of the clinically
540 underexplored IFN-α14 and IFN-β over IFN-α2a to sensitise T-cells for elimination justifies
541 their advancement for clinical trials. In conclusion, combining potent LRAs with
542 immunomodulatory molecules, such as type I IFNs, presents a promising strategy to overcome
543 the intrinsic and/or virus-mediated resistance of HIV-1-reactivating T-cells to NK cell-mediated
544 killing which would be an instrumental step towards effective shock-and-kill cure strategies.
545

546

547

548 **MATERIAL AND METHODS**

549 **Cell lines and primary cells**

550 HEK293T and Tzm-bl cells were obtained from ATCC and the NIH AIDS Reagents Program
551 and maintained in Dulbecco's modified Eagle's medium (DMEM) supplemented with 10%
552 heat-inactivated fetal calf serum (FCS), 100 IU/ml Penicillin/Streptomycin and 2 mM L-
553 Glutamine in a 5% CO_2 atmosphere at 37°C. Jurkat and J1.1 T-cells were obtained from the
554 NIH AIDS Reagents Program and cultivated in RPMI 1640 supplemented with 10% heat-
555 inactivated FCS, 100 IU/ml Penicillin/Streptomycin, 2 mM L-Glutamine, 1x MEM non-essential
556 amino acids and 1 mM sodium pyruvate in a 5% CO_2 atmosphere at 37 °C.
557 Withdrawal of blood samples from healthy human donors and cell isolation were conducted
558 with approval of the local ethics committee (Ethical review committee of Charité Berlin, vote
559 EA4/167/19). Withdrawal of blood samples from aviremic PLHIV and cell isolation were
560 conducted with approval of the local ethics committee (Ethical review committee of Charité
561 Berlin, votes EA2/105/05 and EA2/024/21) in the context of the HIV-1 Seroconverter Study of
562 the Robert-Koch-Institute (77). Available clinical information is indicated in Supplementary
563 Table 1. Human PBMCs, $CD4^+$ T-cells, NK cells and monocytes were isolated from EDTA-
564 anticoagulated blood by Ficoll-Hypaque centrifugation or using the EasySep Direct Human
565 $CD4^+$ T-cell, Human NK cell or Human Monocyte $CD14^+$ Isolation kits (STEMCELL
566 Technologies), respectively. Primary cells were cultured at 10^6 cells/ml in RPMI 1640
567 containing 10% heat-inactivated FCS, 100 IU/ml penicillin/streptomycin, 2 mM L-Glutamine,
568 1% MEM non-essential amino acids and 1 mM sodium pyruvate.

569

570 **Reagents and inhibitors**

571 The following commercial reagents were used throughout this study: Bryostatin I (Sigma
572 Aldrich), CEFX Ultra SuperStim Pool (#PM-CEFX-1, JPT), IFN-α2a (Roche), IFN-β (Roche),

573 IL-2 (Merck), JQ-1 (Sigma Aldrich), Panobinostat (Cayman Chemical), PHA (Thermo
574 Scientific), Romidepsin (Selleckchem), Ruxolitinib (STEMCELL Technologies)
575 Vorinostat/SAHA (Abcam). Efavirenz was obtained from the NIH AIDS Reagent Program.
576 Recombinant IFN-α subtypes 2, 6, 14 and 16 were expressed in *Escherichia coli*, purified by
577 anion-exchange and size exclusion chromatography and tested for absence of endotoxins
578 (50). IFN units were determined using a human retinal pigment epithelial reporter cell line
579 stably expressing a plasmid containing the IFN-stimulated response element driving a
580 luciferase reporter gene.

581 **Treatment of CD4$^+$ T-cells for single cell RNA-sequencing**

582 CD4$^+$ T-cells were mock-treated (0.05% DMSO) or treated with Vorinostat (500 nM),
583 Panobinostat (50 nM) or IL-2 (20 IU/ml) and PHA (1 µg/ml) for 48 hours before subjecting
584 them to the single cell RNA-sequencing pipeline. J1.1 T-cells were treated with 1.6% DMSO
585 (DMSO I), 16000 nM Vorinostat, 0.2% DMSO (DMSO II) or 200 nM Panobinostat for 40 hours
586 before subjecting them to single cell RNA-sequencing.

587 **Single cell RNA-sequencing**

588 Single cell RNA-Seq libraries were prepared with the 10x Genomics platform using the
589 Chromium Next GEM Single Cell 3' Reagent Kits v.3.1 following manufacturer's instructions.
590 Quality control of the libraries were performed with the KAPA Library Quantification Kit and
591 Agilent TapeStation. Libraries were sequenced on a HiSeq4000 using the following
592 sequencing mode: read 1: 28 bp, read 2: 91-100 bp, Index i7: 8 bp. The libraries were
593 sequenced to reach ~20 000 reads per cell.

594 **Single cell RNA-sequencing data analysis**

595 FASTQ files from the sequencing protocol were processed using the Cell Ranger pipeline v
596 3.1.0 (10X Genomics) and further analysed using the Seurat v3.1.4 package (78) in R v3.6 (R
597 Core Team, 2017). Reads from cells isolated from PLHIV were aligned to the human genome
598 (GRCh38), while reads from J1.1 T-cells were aligned to a custom reference consisting of the

599 genomic HIV-1 RNA (LAV-1, GenBank: K02013.1) appended to GRCh38 to allow for capture
600 of viral RNAs. The data was processed using the SCTransform workflow as outlined by the
601 Seurat developers. Cells were clustered using Louvain clustering in a UMAP projection. For
602 the $CD4^+$ T-cells from PLHIV, T-cell subsets were identified based on marker gene expression:
603 T_N cells ($CD3D^+$, $CD8A^-$, $CCR7^+$, $S100A4^{low}$) (39), T_{CM} cells ($CD3D^+$, $CD8A^-$, $CCR7^{low}$,
604 $S100A4^{int}$, $CD62L^{high}$, $GZMA^-$) (79), T_{TM} cells ($CD3D^+$, $CD8A^-$, $CCR7^{low}$, $S100A4^{high}$, $CD62L^{low}$,
605 $GZMA^+$, $GZMB^-$, $GZMH^-$, $PRF1^-$, $GNLY^+$) (80–82), T_{EM} cells ($CD3D^+$, $CD8A^-$, $CCR7^-$,
606 $S100A4^{high}$, $GZMA^+$, $GZMB^+$, $GZMH^+$, $PRF1^+$ $GNLY^+$) (83), T_{EMRA} cells ($CD3D^+$, $CD8A^-$, $CCR7^-$
607 , $S100A4^{high}$, $GZMA^+$, $GZMB^{high}$, $GZMH^+$, $PRF1^{high}$, $GNLY^{high}$, $CCL4^+$) (40,84), T_{REG} cells
608 ($CD3D^+$, $CD8A^-$, $CCR7^{low}$, $S100A4^{high}$, $FOXP3^+$, $IL2RA^+$, $CTLA4^+$) (40,84), T_{EX} cells ($CD3D^+$,
609 $CD8A^-$, $CCR7^-$, $GZMB^+$, $PDCD1^+$, $LAG3^+$) (85). All utilized code is deposited at
610 https://github.com/GoffinetLab/HIV_scRNAseq-CD4-LRA-study. To visualize sequencing
611 coverage of the viral genome in J1.1 T-cells, viral reads were extracted from the bam files of
612 the CellRanger output. These were converted to bigwig files and visualised on tracks using
613 bamCoverage (setting –normalizeUsing RPGC) and pyGenomeTracks from deeptools (86).
614

615 **Principal component analysis (PCA)**

616 PCA was performed with the average expression values of all genes with detectable
617 expression levels of mock-, Vorinostat- and Panobinostat-treated samples. Singular value
618 decomposition (SVD) with imputations was used for calculation of the principal components
619 using ClustVis (https://biit.cs.ut.ee/clustvis/) (87).
620

621 **Differentially expressed genes and pathway analysis**

622 DEGs between individual treatments were identified using the 10x Genomics Loupe Browser
623 (v. 5.0.1.); p-values were adjusted using the Benjamini-Hochberg correction for multiple
624 testing. Pathway analysis was performed with the list of DEGs harbouring p-values <0.05,
625 gene set enrichment analysis (GSEA) was performed using the Pathway Panther database
626 (88–90). The results are described using the Normalised Enrichment Ratio (NER), the

627 enrichment ratio indicates the degree of overrepresentation of a given gene set in the list of
628 DEGs and is normalised to take different gene set sizes into account.
629
630 **Transcription factor activity analysis**
631 Transcription factor activity analysis was performed using the dorothea R package following
632 the guidelines for processing single cell RNA-seq data (91,92), with the following exception.
633 The run_viper function from dorothea was altered to use the top 40,000 most variable genes,
634 as determined by the FindVariableFeatures function from Seurat. Utilised code is available at
635 https://github.com/GoffinetLab/HIV_scRNAseq-CD4-LRA-study.
636
637 **Module scores**
638 The IFN signalling pathway (R-HSA-913531) and TCR signalling pathway (R-HSA-202403)
639 gene sets from the Reactome database (93) were retrieved from the Molecular Signatures
640 Database (MSigDB) (94). Cells were scored based on their expression of these genes using
641 the AddModuleScore function in Seurat. They are referred to as the IFN signalling module and
642 T-cell activation module scores as the pathways include genes canonically involved in
643 response to IFN signalling and TCR-mediated T-cell activation, respectively.

644 **Flow cytometry**
645 PBS-washed cells were immunostained for individual surface proteins using the following
646 antibodies: anti-BST2/Tetherin-BV421 (#566381; BD), anti-CCR5/CD195-FITC (#555992; BD
647 Biosciences), anti-CCR7/CD197-PE (#552176; BD Biosciences), anti-CD107a-BV421
648 (#562623; BD), anti-CD14-PE (#555398; BD), anti-CD16-FITC (#360716; Biolegend), anti-
649 CD3-FITC (#561807; BD Biosciences), anti-CD4-APC (#555349; BD Biosciences), anti-
650 CD25-APC (#340907; BD Biosciences), anti-CD45RA-FITC (#335039; BD Biosciences), anti-
651 CD45RO-APC (#340438; BD Biosciences), anti-CD56-APC (#318310; Biolegend), anti-
652 CD62L-FITC (#304804; Biolegend), anti-CD69-APC (#340560; BD Biosciences), anti-
653 CXCR4/CD184-APC (#555976; BD Biosciences), anti-HLA-DR-FITC (#556643, BD

654 Biosciences), anti-IL7R/CD127-PE (#557938; BD), anti-PD-1/CD279-PE (#21272794;
655 ImmunoTools) and anti-TIM-3/CD366-FITC (#345022; Biolegend). For intracellular
656 immunostaining, PBS-washed cells were PFA-fixed for 90 minutes and immunostained with
657 the following antibodies diluted in 0.1% Triton X-100 in PBS: anti-HIV-1-core-antigen-FITC or
658 -PE (#6604665 or #6604667; Beckman Coulter), rabbit-anti-human-MX1/2 (#sc-166412;
659 Santa Cruz Biotechnology). A goat-anti-rabbit IgG conjugated to Alexa Fluor 647 (#A27040;
660 Thermo Fisher) was used as a secondary antibody. Cell viability was analysed using the Dead
661 Cell Apoptosis Kit for Flow Cytometry from Invivogen (#V13242), with early apoptotic cells
662 scoring Annexin V-positive and late apoptotic cells scoring Annexin V- and propidium iodide
663 (PI)-positive. Data acquisition and analysis was conducted using a FACS Celesta device
664 (Becton Dickinson, Franklin Lakes, New Jersey, USA) with FlowJo (v.10.7.1).
665

666 **T-cell activation assays**

667 $CD4^+$ T-cells were isolated from healthy donors and pre-incubated with Vorinostat (500 nM),
668 Panobinostat (50 nM), or left mock-treated (0.05% DMSO) for 16 hours followed by stimulation
669 with a peptide pool of a broad range of HLA-subtypes and infectious agents (CEFX Ultra
670 SuperStim Pool; JPT) (1 µg/ml) and 1 µg/ml mouse-anti-human CD28 antibody (#556620; BD
671 Biosciences), or IL-2 (20 IU/ml) and PHA (1 µg/ml). T-cell activation and exhaustion was
672 quantified by flow cytometry 48 hours post-stimulation.

673 **HIV-1 reactivation assays in J1.1 T-cells**

674 J1.1 T-cells were PBS-washed, resuspended in supplemented RPMI and incubated with
675 Panobinostat (50 nM), Vorinostat, (5000 nM), Romidepsin (50 nM), Bryostatin (20 nM), JQ1
676 (5000 nM) or the corresponding volume of DMSO, if not otherwise stated for 48 hours. In some
677 assays, T-cells were co-treated or pre-treated for 24 hours with individual IFNs at indicated
678 concentrations.

679 **Quantitative RT-Q-PCR**

680 Total RNA extraction using the Direct-zol RNA extraction kit (Zymo) including DNase treatment
681 to remove residual DNA contaminations, was followed by cDNA synthesis (NEB, Invitrogen)
682 and quantification of relative mRNA levels using a LightCycler 480 Instrument II (Roche) and
683 Taq-Man PCR technology. For human *IFIT1* and *MX2*, a premade primer-probe kit was
684 purchased from Applied Biosystems (Assay ID: Hs01911452_s1; Hs01550813_m1;
685 respectively. Relative mRNA levels were determined in multiplex reactions using the ΔΔCt
686 method and human *RNASEP* (#4316844; Applied Biosystems) as internal reference. Data
687 analysis was performed using LightCycler Software 4.1 (Roche).
688
689 **Immunoblotting**
690 For immunoblotting, cells were lysed using the M-PER mammalian protein extraction reagent
691 (Thermo Fisher Scientific) following manufacturer's recommendations. Cell cultures
692 supernatants were centrifuged over a 20% sucrose cushion at 20,000 x g, for 60 mins at 4°C,
693 resuspended in 1x SDS buffer at heat-inactivated for 10 mins at 95°C. Samples were run on
694 a 10% SDS-PAGE, transferred onto nitrocellulose membranes using a semi-dry transfer
695 system (Bio-Rad Laboratories) and membranes were blocked with 5% milk in TBS for one
696 hour before incubation with the primary antibody at 4°C overnight. The following primary
697 antibodies were used: anti-90K/LGALS3BP (#AF2226: R&D Systems), anti-BST2/Tetherin
698 (#390719; Santa Cruz), anti-ERK2/MAPK (#sc-153; Santa Cruz) anti-GAPDH (#NB300-221,
699 Novus Biologicals), anti-HIV-1 p24 (#11-327; ExBio), anti-HIV-1 gp120 (provided by Valerie
700 Bosch), anti-IFIT1 (#TA500948; OriGene), anti-IFITM-3 (#AP1153a; Abgent), anti-ISG15
701 (#166755; Santa Cruz) and anti-MX2 (#sc166412; Santa Cruz). Secondary antibodies
702 conjugated to Alexa680 or Alexa800 fluorescent dyes were used for detection and
703 quantification by the Odyssey Infrared Imaging System (LI-COR Biosciences).
704 Release of HIV-1 p24 capsid was quantified by detecting p24 as described above in
705 supernatant and cell samples from corresponding cell cultures and dividing the p24 signal
706 intensity from supernatants by the sum of p24 intensities from both fractions.
707

708 **Tzm-bl HIV-1 infectivity assay**

709 To quantify infectivity released in supernatant, 30,000 Tzm-bl cells per 96-well were pre-
710 treated with 10 µM of the JAK/STAT inhibitor Ruxolitinib for 16 hours to minimise the influence
711 of potentially transferred IFNs from the tested supernatants. Then, cells were infected with
712 HIV-1 for 48 hours before luminometric quantification of luciferase activity using the Luciferase
713 Assay System (Promega).

714 **HIV-1 Env cell surface staining**

715 To quantify HIV-1 Env cell surface expression, broadly neutralising antibodies 3BNC117
716 (ARP-12474), 10-1074 (ARP-12477) and PG16 (ARP-12150) were obtained from the NIH HIV
717 Reagents Program. PBS-washed cells were immunostained with a cocktail of 5 µg/ml of each
718 antibody for 30 mins at 4°C, followed by PBS washing and immunostaining with secondary
719 AlexaFluor633 anti-human antibodies (Thermo Fisher Scientific, #A-21091) for 30 mins at 4°C
720 in the dark. Samples were PBS-washed and fixed with 4% PFA for 90 minutes. Samples were
721 acquired and analysed on a FACS Celesta machine (BD Biosciences) and FlowJo Software
722 (V.10.7.1), respectively.

723

724 **Thin section electron microscopy**

725 Infected T-cells were fixed with 2.5% glutaraldehyde in 0.05 M Hepes buffer (pH:7.2) and
726 incubated at room temperature for two hours. Afterwards, µ-Dishes were filled with the fixative
727 buffer and cells were embedded in the chambers by using Epon resin (protocol with tannic
728 acid and uranyl acetate block contrasting (95). Thin sections (60-70 nm thick) were produced
729 with an ultramicrotome, contrasted with uranyl acetate and lead citrate and investigated with
730 a transmission electron microscope (JEM-2100, Jeol) operated at 200 kV. Images were
731 recorded using a side-mounted CCD camera (Veleta, EMSIS) with 2048x2048 pixels.

732

733

734

735 **Antibody-dependent cellular cytotoxicity (ADCC) assay**

736 ADCC assays were adapted from previous reports (96). Briefly, J1.1 T-cells were treated as
737 described above for 48 hours, before washing and staining with green CellTracker (#C2925,
738 Thermo Fisher Scientific), following manufacturer's recommendations. Labelled J1.1 T-cells
739 were then co-cultured with freshly isolated PBMCs (or NK cells or monocytes where indicated)
740 at a 1:1 ratio in a 96-well U-bottom plate in the presence of indicated dilutions of serum from
741 PLHIV (ARP-3957; obtained from the NIH HIV Reagents Program). A separate well without
742 serum was set up for each co-culture condition in parallel. The plates were then centrifuged
743 for one min, 300 x *g* and then incubated at 37°C, 5% CO_2. After four hours, co-cultures were
744 PBS-washed, fixed with 4% PFA, immunostained for intracellular HIV-1 p24 expression and
745 p24 CA-positive J1.1 T-cells were quantified by flow cytometry. Percent of ADCC was
746 calculated using this formula (see also **Sup. Fig. 8**):

747 $$\% \, ADCC$$

748 $$= \frac{p24 - positive\ J1.1\ cells\ (without\ sera)\ -\ p24 - positive\ J1.1\ cells\ (with\ sera)}{p24 - positive\ J1.1\ cells\ (without\ sera)}\ x\ 100$$

749

750 **NK cell activation and CD107a degranulation assay**

751 NK cell activation and degranulation activity in PBMCs co-cultured with reactivated J1.1 T-
752 cells was analysed through CD16 and CD107a immunostaining of NK cells. ADCC assays
753 were performed as described above with the following modifications (97): Co-cultures were
754 supplemented with a 1:20 dilution of anti-CD107a-BV421 antibodies. After one hour of
755 incubation, a final concentration of 10 µg/ml Brefeldin A and 6 µg/ml Golgi-Stop (BD
756 Biosciences) were added, preventing the exocytosis of cytokine-containing vesicles, and the
757 acidification of endocytic vesicles and CD107a protein degradation, respectively. Co-cultures
758 were incubated for another three hours at 37°C, 5% CO_2, before immunostaining for CD16
759 and CD56 cell surface expression. CD16 and CD107a expression was assessed by flow
760 cytometry specifically in CD56-positive NK cell populations (see also **Sup Fig. 9**).

761

762 **Live-cell imaging of J1.1 T-cell/NK cell co-cultures**

763 To analyse the dynamics of NK cell-mediated ADCC against reactivating J1.1 T-cells, live cell
764 imaging of indicated co-cultures was performed. J1.1 T-cell cultures treated with Panobinostat
765 or Panobinostat/IFN-α2a for 48 hours were individually labelled with CellTracker™ Green-
766 CFMDA or CellTracker™ Deep Red CellTracker (both Thermo Fisher Scientifics).
767 Panobinostat-treated, Panobinostat/IFN-α2a-treated J1.1 T-cells and NK cells were co-
768 cultured at a 1:1:1 ratio in the presence of 1:100 dilution of sera from PLHIV and the
769 LIVE/DEAD Aqua Dead Cell dye (Thermo Fisher Scientific, #L34965) to assess dying cells.
770 The dead cell dye reacts with free amids in the cellular cytosol, thus specifically staining cells
771 with porous membranes as an early surrogate of cell death. Co-cultures were monitored with
772 a Zeiss LSM800 Airyscan Confocal Microscope in a 37°C, 5% CO_2 atmosphere with images
773 being acquired every three minutes for a total of four hours. Images were analysed and
774 merged using Zeiss ZEN Blue (V3.3).

775

776 **Data presentation and statistical analysis**

777 Graphs and figures were generated using Graphpad Prism 9 (v.9.5.1) and Adobe Illustrator
778 2021. Heatmaps were generated using the ClustVis web tool (https://biit.cs.ut.ee/clustvis/)
779 with unit variance scaling for rows (87). If not otherwise stated, bars or circles represent the
780 mean of the indicated number of experiments and error bars indicate the S.E.M. Statistical
781 significance for paired data sets were tested using Graphpad Prism 9 and paired student's t-
782 testing, p-values ≤ 0.05 were considered significant and displayed in the figures as follows: p
783 < 0.05 *; p < 0.01 ** or p < 0.001 ***. p-values ≥ 0.05 were considered not significant (n.s.).
784 Pearson's correlation analyses were performed for the indicated datasets with pearson
785 correlation coefficients and two-tailed p-values being displayed.

786 **Data availability**

787 The single cell RNA-sequencing data will be deposited at the Gene Expression Omnibus
788 (GEO) database (accession number #).

789

790 **ACKNOWLEDGEMENTS**

791 We thank the PLHIV who agreed to participate in the Seroconverter Study and the uninfected
792 donors to provide their blood for research. We thank Valerie Bosch and the NIH AIDS
793 Research & Reference Reagent Program for providing essential reagents. We thank the
794 Genomics Platform of the Berlin Institute of Health for next-generation sequencing. This work
795 was supported by funding to C.G. by Berlin Institute of Health (BIH); by Hector Foundation,
796 project M2101; by DFG priority program 1923 "Innate Sensing and Restriction of
797 Retroviruses," grant GO2153/4); by DZIF, TTU HIV, grant 04.820 to C.G. and by a
798 Professorship Award (APR9/1017) of the Academy of Medical Sciences awarded to C.G. We
799 thank Christian Drosten for constant support. A.P. is supported by the Brazilian Federal
800 Foundation for Support and Evaluation of Graduate Education, CAPES. J.K. is supported by
801 the Center of Infection Biology and Immunity (ZIBI) and Charité PhD Program.

802

803 **AUTHOR CONTRIBUTIONS**

804 JP, AJP, JJ, LM, JF, TS, performed experiments.
805 JP, DP, AJP, EW, LM, JF, TS, CF, SV, MS analysed data.
806 UK, BGB, KM, NB, LL, AT, KS provided essential resources.
807 AT, SS, UD, MiL, NB, MaL, CG supervised.
808 CG acquired funding and managed the project.
809 JP, DP, CG wrote the manuscript.

810 **Declaration of conflicts of interest**

811 None.

812 **FIGURES**

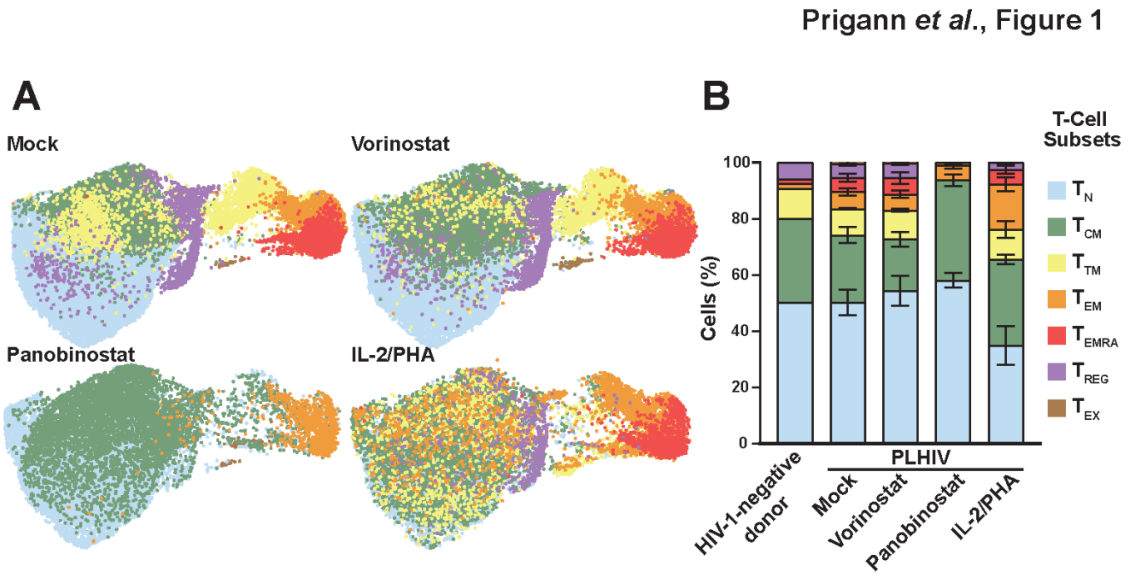

813

814 **Figure 1. Panobinostat treatment modulates expression of CD4⁺ T-cell subset-specific**

815 **markers**

816 (**A**) Combined UMAP plot of CD4⁺ T-cell cultures from three PLHIV, separated by treatment

817 and coloured by T-cell subset.

818 (**B**) Percentages of indicated CD4⁺ T-cell subsets.

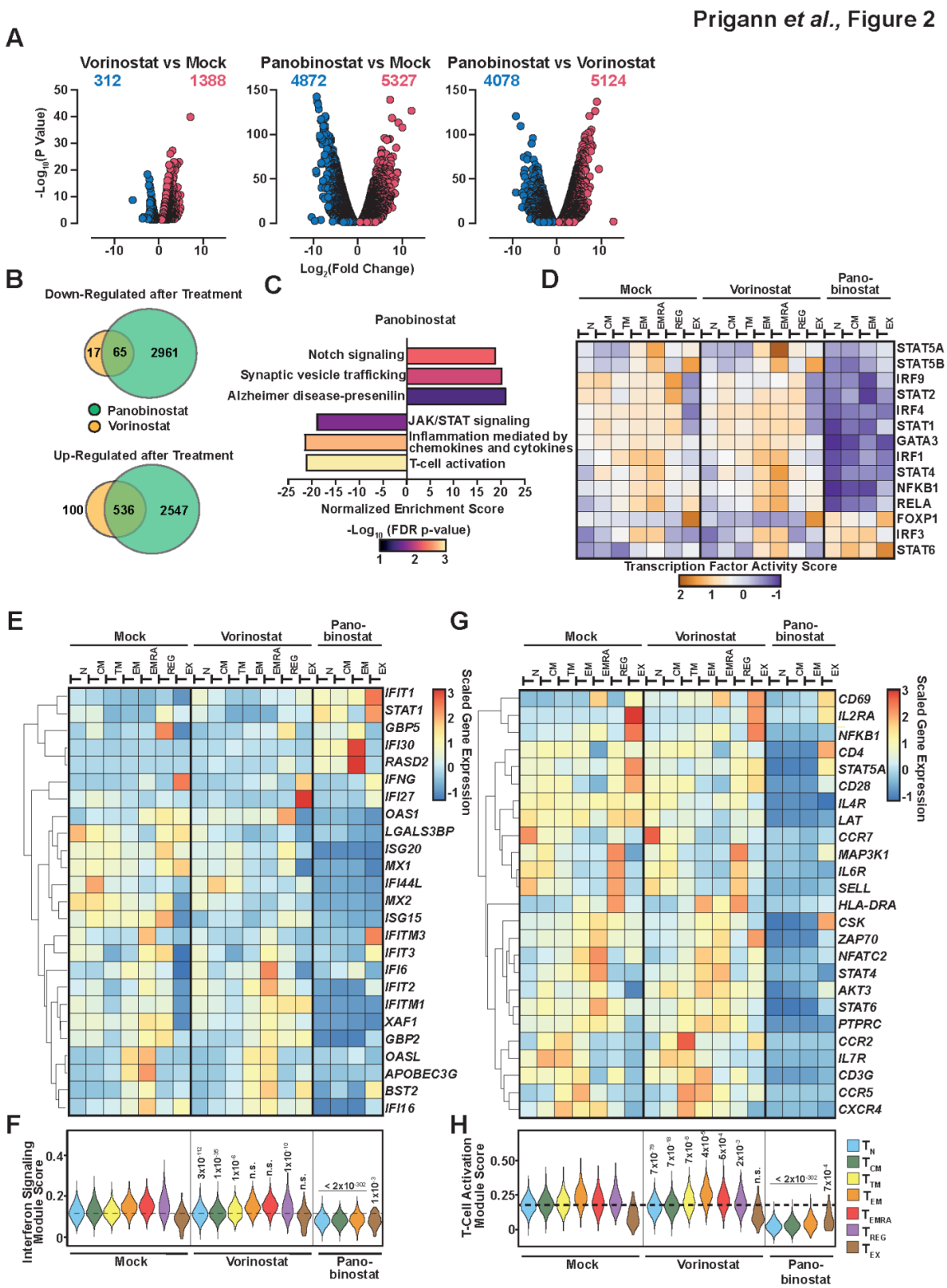

Figure 2. Panobinostat treatment induces broad transcriptional down-modulation of genes involved in T-cell signalling and a subset of genes implicated in innate immunity

822 (**A**) Volcano plots showing DEGs with a p-value < 0.05.

823 (**B**) Overlap of genes significantly up- or down-regulated (p-value < 0.05, fold change > 2) in
824 Vorinostat and Panobinostat-treated samples compared to mock treatment.

825 (**C**) Pathway analysis of DEGs (p-value < 0.05) after Panobinostat treatment. Shown is the
826 Normalised Enrichment Ration (NER), representing the degree of overrepresentation of a
827 given gene set in the DEG list. Colours indicate the $-Log_{10}$(FDR p-value).

828 (**D**) Transcription factor activity analysis of selected transcription factors in the indicated T-cell
829 subsets.

830 (**E**) Heatmap showing scaled average expression of selected ISGs in the indicated T-cell
831 subsets. Genes are ordered based on correlation, clustering is indicated with lines on the left.

832 (**F**) Average IFN signalling module score in the indicated T-cell subsets. Dashed line shows
833 the average module score of mock-treated T_N-cells. Numbers indicate the p-value calculated
834 using Wilcoxon signed-rank testing for each subset from the LRA-treated samples compared
835 to the same subset of the mock-treated samples.

836 (**G**) Heatmap showing scaled average expression of selected genes required for T-cell-
837 mediated immunity in the indicated T-cell subsets. Genes are ordered based on correlation,
838 clustering is indicated with lines on the left.

839 (**H**) Average T-cell activation module score in the indicated T-cell subsets. Dashed line shows
840 the average module score of mock-treated T_N-cells. Numbers indicate the p-value calculated
841 using Wilcoxon signed-rank testing for each subset from the LRA-treated samples compared
842 to the same subset of the mock-treated samples.

843

Prigann *et al.*, Figure 3

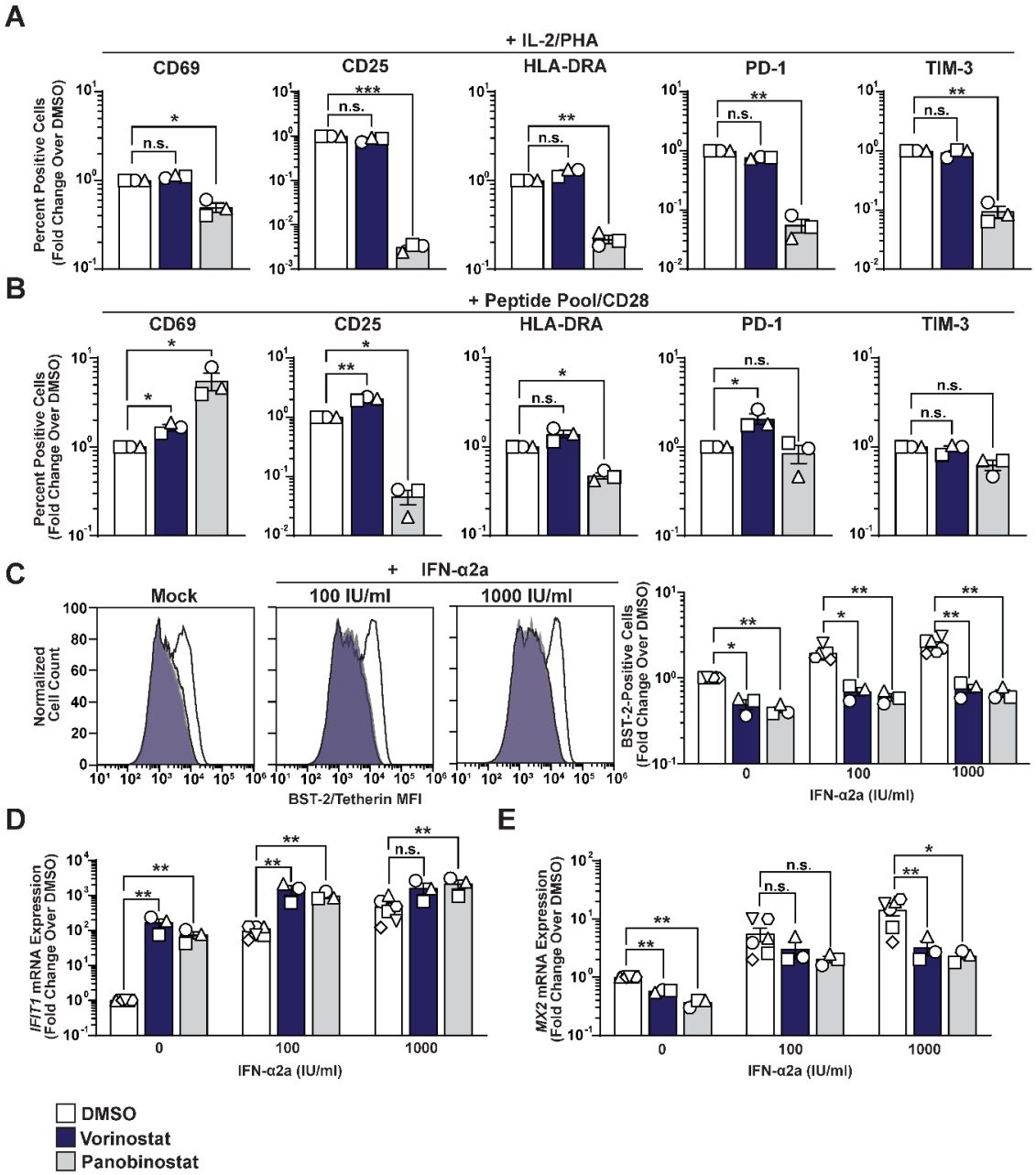

Figure 3. HDAC inhibition imposes a block to CD4⁺ T-cell activation and type I IFN signalling

CD4⁺ T-cells from uninfected donors were either pretreated with 0.5% DMSO, 500 nM Vorinostat or 50 nM Panobinostat for 16 hours, followed by:

(**A**) Stimulation with a peptide pool and anti-CD28 antibody for 48 hours

(**B**) Stimulation with IL-2/PHA for 48 hours

851 followed by analysis of CD69, CD25, HLA-DR, TIM-3 and PD-1 cell surface expression by flow
852 cytometry. Shown are data from cells from three donors.
853 $CD4^+$ T-cells from uninfected donors were treated with 0.5% DMSO, 8000 nM Vorinostat or
854 50 nM Panobinostat in combination with increasing concentrations of IFN-α2a for 48 hours
855 before analysing:
856 (**C**) BST2 cell surface levels by flow cytometry. Shown are representative histograms from one
857 experiment (left panel) and quantification from experiments with cells from three donors.
858 (**D**) *IFIT1* mRNA expression by RT-Q-PCR. Shown are data from cells from 3-6 donors.
859 (**E**) *MX2* mRNA expression by RT-Q-PCR. Shown are data from cells from 3-6 donors.
860
861
862

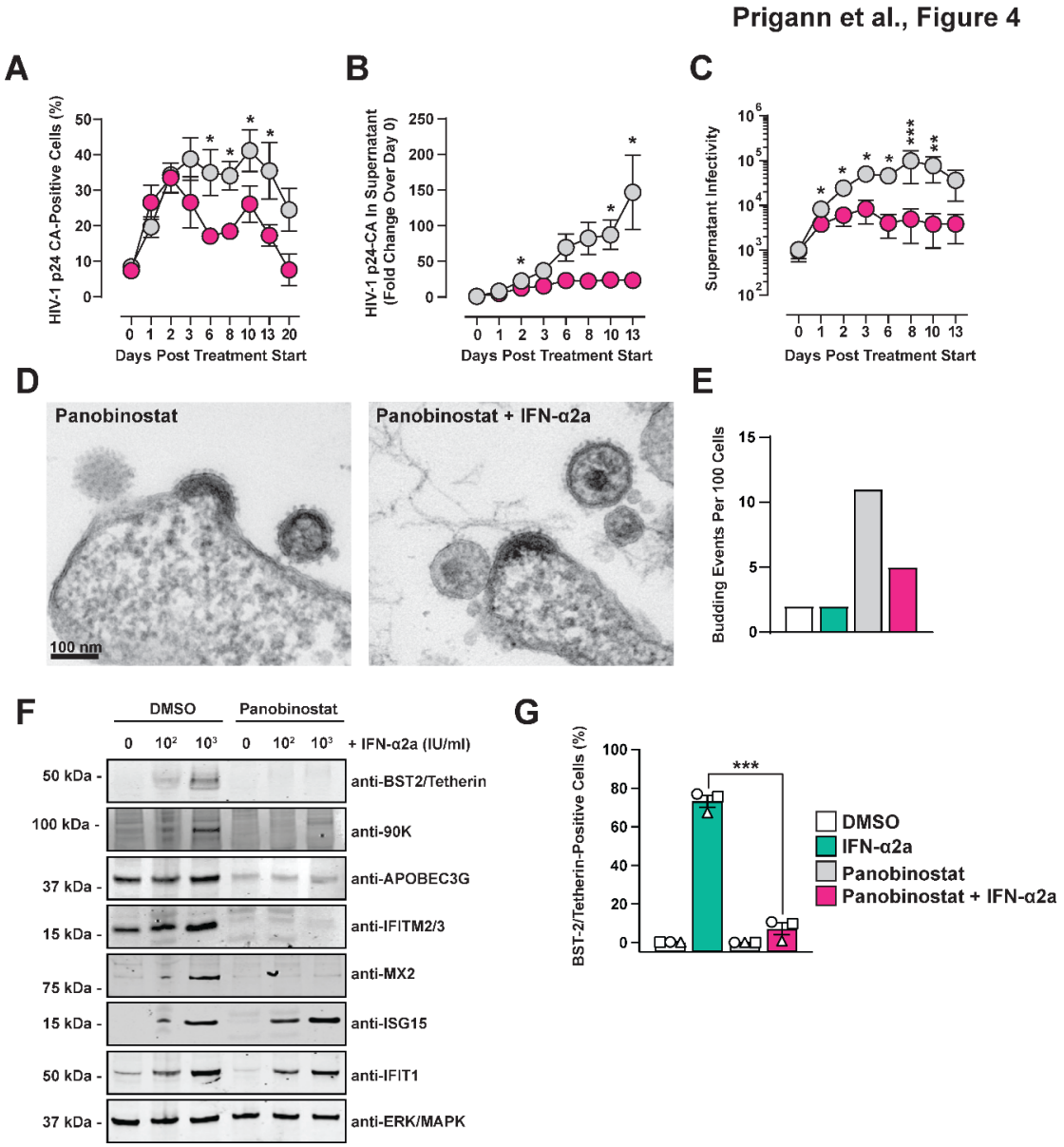

Figure 4. Addition of IFN-α2a to Panobinostat results in a tetherin-independent pre-budding defect

J1.1 T-cells received a single dose of 50 nM Panobinostat alone or in combination with 100 IU/ml IFN-α2a. At indicated time points, samples were analysed for:

(**A**) Cell-associated HIV-1 p24 capsid expression by flow cytometry

(**B**) HIV-1 p24 capsid abundance in cell culture supernatant by immunoblotting.

(**C**) Infectivity in cell culture supernatant using the Tzm-bl reporter cell assay.

(**D**) Representative electron micrographs of reactivated J1.1 T-cells 48 hours post reactivation. Scale bar indicates 100 nm.

(**E**) Electron microscopy-based quantification of budding events per 100 cells analysed.

(**F**) Immunoblot analysis of selected ISG expression in J1.1 T-cells following 48 hours of indicated treatment.

(**G**) J1.1 T-cell surface BST-2/Tetherin expression 48 hours following treatment start.

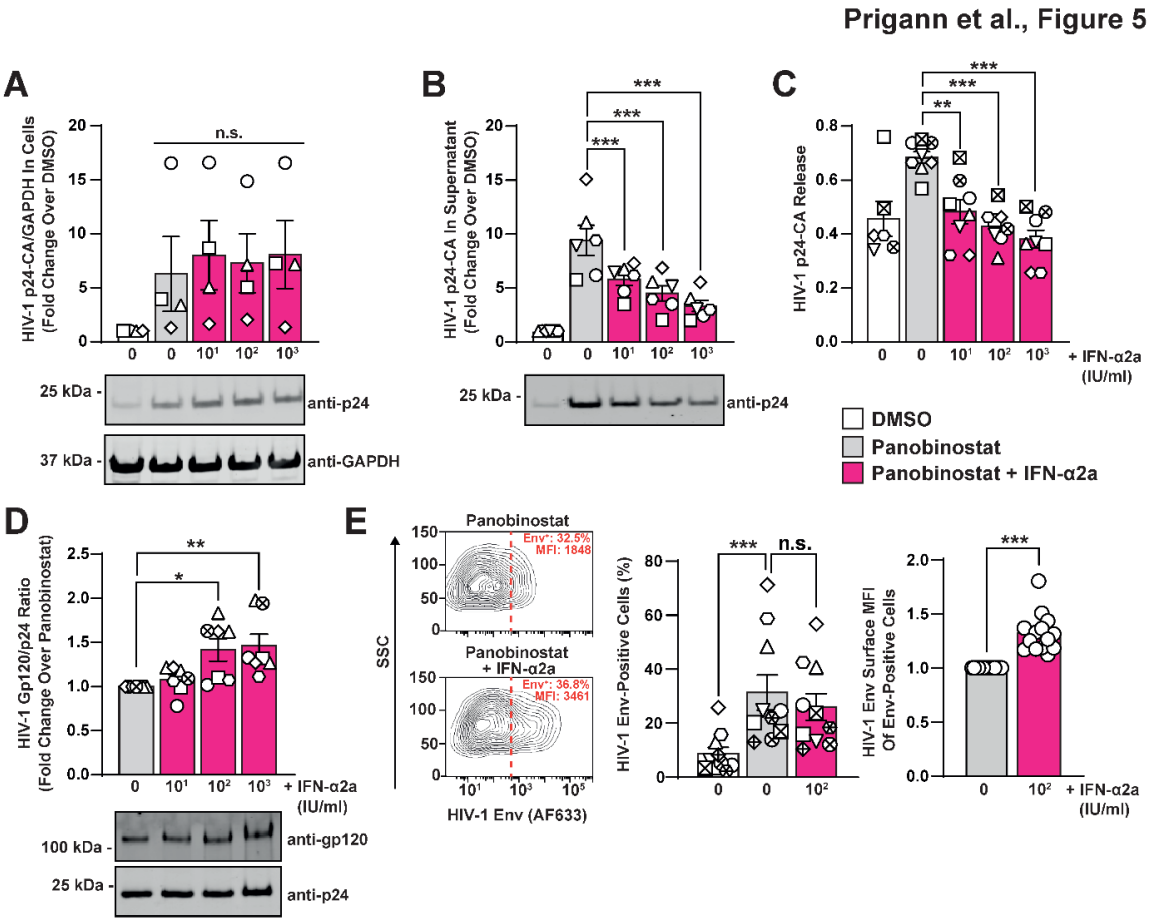

887 **Figure 5. IFN-induced virus pre-budding block is accompanied by accumulation of HIV-**
888 **1 Env on cellular and viral membranes**
889 J1.1 T-cells were treated with 50 nM Panobinostat in the presence or absence of indicated
890 concentrations of IFN-α2a for 48 hours. Cells and corresponding supernatants were analysed
891 for:
892 (**A**) Relative expression of cell-associated HIV-1 p24-CA by immunoblotting, normalised to
893 cellular GAPDH.
894 (**B**) Relative abundance of extracellular HIV-1 p24-CA by immunoblotting, normalised to
895 corresponding DMSO controls.
896 (**C**) Virus release was quantified by normalising extracellular HIV-1 p24-CA signal intensity to
897 the sum of cell-associated and secreted HIV-1 p24-CA.
898 (**D**) HIV-1 gp120 signal intensities from cell culture supernatants were quantified by
899 immunoblotting and normalised to corresponding HIV-1 p24-CA levels.
900 (**E**) Representative dot plots of intact J1.1 T-cells immunostained for surface HIV-1 Env with
901 indicated percentage of Env-positive cells and mean fluorescence intensity (MFI) of Env-
902 positive cells. Quantification of HIV-1 Env-positive cells (middle) and the fold change of Env
903 MFI in Env-positive cells over Panobinostat-treated cells (right) are shown for multiple
904 experimental replicates.
905 Experiments were conducted in 5-13 independent replicates.
906
907
908
909
910
911
912
913
914

915

916

917

918

919

920

921

922

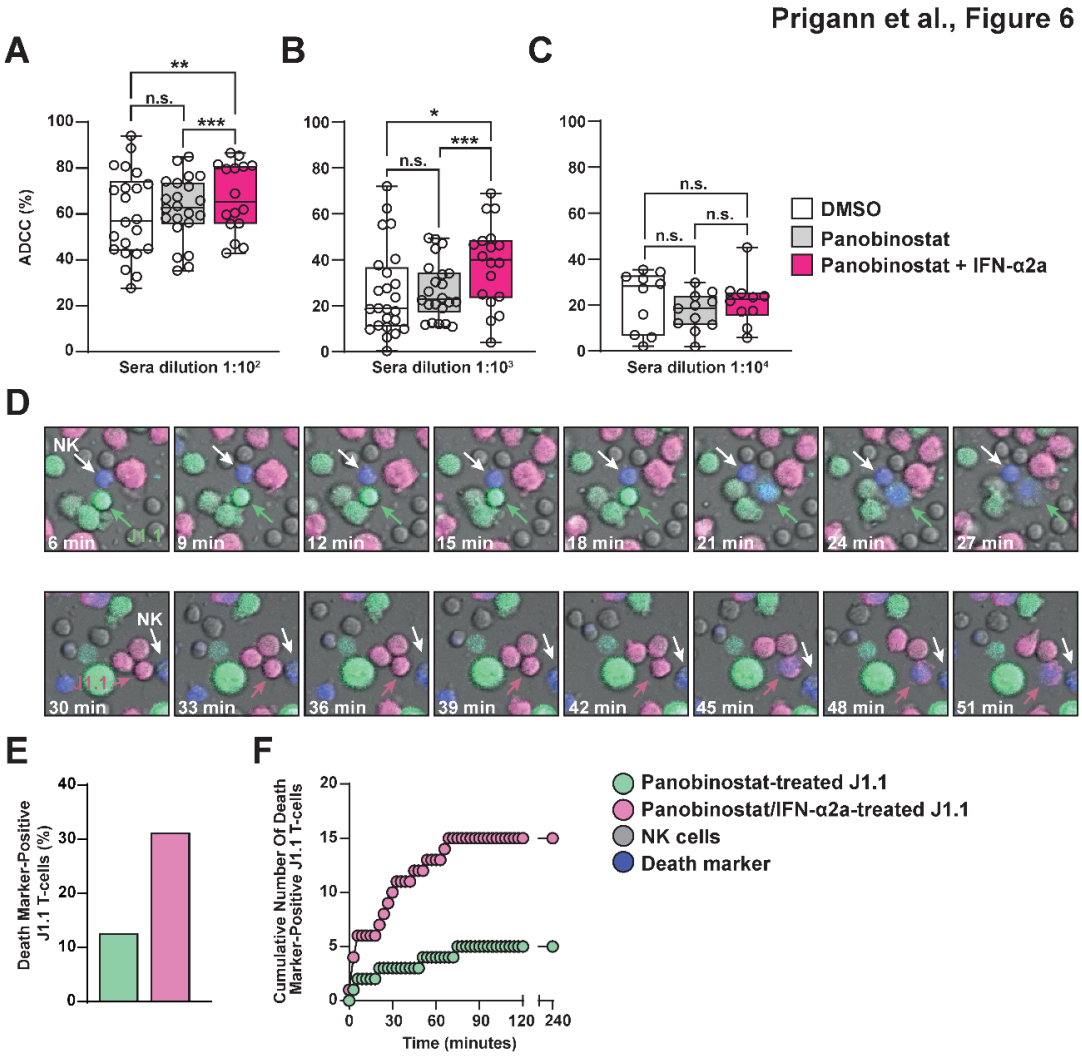

923

924 **Figure 6. Addition of IFN-α2a to Panobinostat enhances the susceptibility of HIV-1-**

925 **reactivating cells to antibody-dependent cellular cytotoxicity via NK cells**

926 (**A-C**) J1.1 T-cells were treated with DMSO, 50 nM Panobinostat alone or in combination with
927 100 IU/ml IFN-α2a for 48 hours before culturing them with PBMCs in the presence of indicated
928 dilutions of sera from PLHIV. Following four hours of co-culture, cells were immunostained for
929 cell-associated HIV-1 p24 CA expression and percentage of ADCC was calculated based on
930 the quantitative difference of HIV-1-p24-positive cells in the identical co-culture merely
931 differing in the presence or absence of serum. Boxes extend from the 25th to 75th percentiles
932 of 10-24 repetitions, the lines indicate the median, error bars represent the minimum and
933 maximum values obtained and symbols the individual experimental replicates.
934 (**D**) - (**F**) J1.1 T-cells were treated with 50 nM Panobinostat alone or in combination with 100
935 IU/ml IFN-α2a for 48 hours and individually stained with CellTracker™ Green-CFMDA and
936 Deep Red, respectively. Stained J1.1 T-cells were co-cultured with non-stained, freshly
937 isolated NK cells at a 1:1:1 ratio in the presence of a cell death marker (blue) and a 1:100
938 dilution of sera from PLHIV containing anti-HIV-1 Env antibodies. The co-culture was
939 monitored using live-cell imaging for four hours with images acquired every three minutes.
940 (**D**) Representative time series of NK cell/J1.1 T-cell interactions and subsequent killing of J1.1
941 T-cells.
942 (**E**) Percentage of dead J1.1 T-cells after four hours, normalised to the number of living J1.1
943 T-cells in the first frame.
944 (**F**) Cumulative number of death marker-positive cells in each J1.1 T-cell population over time.
945
946
947
948
949
950
951
952
953

954

955

956

957

958

959

960

Prigann et al., Figure 7

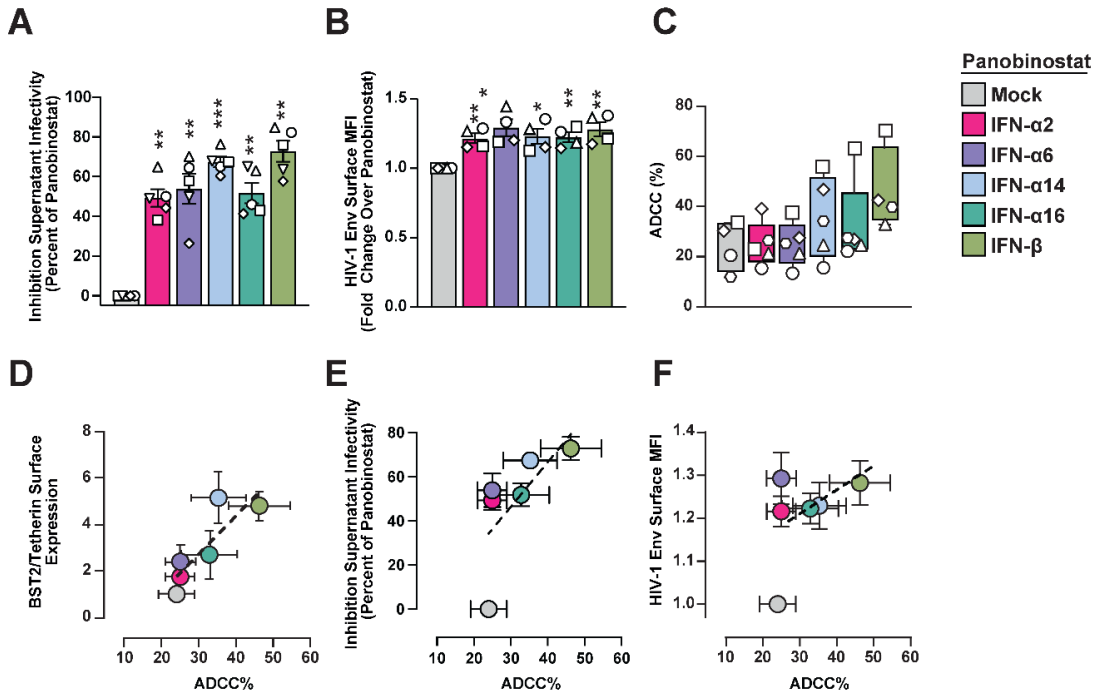

961

962 **Figure 7. The ability to restrict HIV-1 budding and facilitate elimination of HIV-1-positive**

963 **T-cells is type I IFN protein-specific**

964

965 J1.1 T-cells were treated with 50 nM Panobinostat in combination with 100 IU/ml of the

966 indicated IFNs for 48 hours.

967 (**A**) Inhibition of supernatant infectivity was quantified using a Tzm-bl reporter assay, values

968 were normalised to the corresponding Panobinostat-only conditions.

969 (**B**) Fold change of Env MFI in Env-positive cells over Panobinostat-treated cells.

970 (**C**) J1.1 T-cells were co-cultured with PBMCs in the presence of serum from PLHIV (dilution
971 1:1000) to monitor and quantify ADCC.
972 (**D**) - (**F**) Pearson's correlation analysis of ADCC % with BST2/Tetherin surface expression,
973 supernatant infectivity and HIV-1 Env surface expression levels.
974
975
976
977
978 **REFERENCES**

979 1. Chun TW, Carruth L, Finzi D, Shen X, DiGiuseppe JA, Taylor H, et al. Quantification of
980 latent tissue reservoirs and total body viral load in HIV-1 infection. Nature. 1997 May
981 8;387(6629):183–8.
982 2. Chun TW, Stuyver L, Mizell SB, Ehler LA, Mican JA, Baseler M, et al. Presence of an
983 inducible HIV-1 latent reservoir during highly active antiretroviral therapy. Proc Natl Acad
984 Sci U S A. 1997 Nov 25;94(24):13193–7.
985 3. Finzi D, Hermankova M, Pierson T, Carruth LM, Buck C, Chaisson RE, et al.
986 Identification of a reservoir for HIV-1 in patients on highly active antiretroviral therapy.
987 Science. 1997 Nov 14;278(5341):1295–300.
988 4. Wong JK, Hezareh M, Günthard HF, Havlir DV, Ignacio CC, Spina CA, et al. Recovery of
989 replication-competent HIV despite prolonged suppression of plasma viremia. Science.
990 1997 Nov 14;278(5341):1291–5.
991 5. Finzi D, Blankson J, Siliciano JD, Margolick JB, Chadwick K, Pierson T, et al. Latent
992 infection of CD4+ T cells provides a mechanism for lifelong persistence of HIV-1, even in
993 patients on effective combination therapy. Nat Med. 1999 May;5(5):512–7.
994 6. Siliciano JD, Kajdas J, Finzi D, Quinn TC, Chadwick K, Margolick JB, et al. Long-term
995 follow-up studies confirm the stability of the latent reservoir for HIV-1 in resting CD4+ T
996 cells. Nat Med. 2003 Jun;9(6):727–8.
997 7. Deeks SG, Archin N, Cannon P, Collins S, Jones RB, de Jong MAWP, et al. Research
998 priorities for an HIV cure: International AIDS Society Global Scientific Strategy 2021. Nat
999 Med. 2021 Dec;27(12):2085–98.
1000 8. Kim Y, Anderson JL, Lewin SR. Getting the "kill" into "shock and kill": strategies to
1001 eliminate latent HIV. Cell Host Microbe. 2018 Jan 10;23(1):14–26.
1002 9. Margolis DM, Garcia JV, Hazuda DJ, Haynes BF. Latency reversal and viral clearance to
1003 cure HIV-1. Science. 2016 Jul 22;353(6297):aaf6517.
1004 10. Van Lint C, Emiliani S, Ott M, Verdin E. Transcriptional activation and chromatin
1005 remodeling of the HIV-1 promoter in response to histone acetylation. EMBO J. 1996 Mar
1006 1;15(5):1112–20.
1007 11. Archin NM, Keedy KS, Espeseth A, Dang H, Hazuda DJ, Margolis DM. Expression of
1008 latent human immunodeficiency type 1 is induced by novel and selective histone
1009 deacetylase inhibitors. AIDS. 2009 Sep 10;23(14):1799–806.
1010 12. Søgaard OS, Graversen ME, Leth S, Olesen R, Brinkmann CR, Nissen SK, et al. The
1011 Depsipeptide Romidepsin Reverses HIV-1 Latency In Vivo. PLoS Pathog. 2015
1012 Sep;11(9):e1005142.
1013 13. Williams SA, Chen LF, Kwon H, Fenard D, Bisgrove D, Verdin E, et al. Prostratin
1014 antagonizes HIV latency by activating NF-kappaB. J Biol Chem. 2004 Oct
1015 1;279(40):42008–17.

1016 14. Beans EJ, Fournogerakis D, Gauntlett C, Heumann LV, Kramer R, Marsden MD, et al.
1017 Highly potent, synthetically accessible prostratin analogs induce latent HIV expression in
1018 vitro and ex vivo. Proc Natl Acad Sci. 2013 Jul 16;110(29):11698–703.
1019 15. Gutiérrez C, Serrano-Villar S, Madrid-Elena N, Pérez-Elías MJ, Martín ME, Barbas C, et
1020 al. Bryostatin-1 for latent virus reactivation in HIV-infected patients on antiretroviral
1021 therapy. AIDS Lond Engl. 2016 Jun 1;30(9):1385–92.
1022 16. Zhu J, Gaiha GD, John SP, Pertel T, Chin CR, Gao G, et al. Reactivation of latent HIV-1
1023 by inhibition of BRD4. Cell Rep. 2012 Oct 25;2(4):807–16.
1024 17. Nixon CC, Mavigner M, Sampey GC, Brooks AD, Spagnuolo RA, Irlbeck DM, et al.
1025 Systemic HIV and SIV latency reversal via non-canonical NF-κB signalling in vivo.
1026 Nature. 2020 Feb;578(7793):160–5.
1027 18. Thibault S, Imbeault M, Tardif MR, Tremblay MJ. TLR5 stimulation is sufficient to trigger
1028 reactivation of latent HIV-1 provirus in T lymphoid cells and activate virus gene
1029 expression in central memory CD4+ T cells. Virology. 2009 Jun 20;389(1–2):20–5.
1030 19. Novis CL, Archin NM, Buzon MJ, Verdin E, Round JL, Lichterfeld M, et al. Reactivation
1031 of latent HIV-1 in central memory $CD4^+$ T cells through TLR-1/2 stimulation.
1032 Retrovirology. 2013 Oct 24;10:119.
1033 20. Abner E, Jordan A. HIV “shock and kill” therapy: In need of revision. Antiviral Res. 2019
1034 Jun;166:19–34.
1035 21. Arandjelovic P, Kim Y, Cooney JP, Preston SP, Doerflinger M, McMahon JH, et al.
1036 Venetoclax, alone and in combination with the BH3 mimetic S63845, depletes HIV-1
1037 latently infected cells and delays rebound in humanized mice. Cell Rep Med. 2023 Sep
1038 19;4(9):101178.
1039 22. Collins DR, Gaiha GD, Walker BD. CD8+ T cells in HIV control, cure and prevention. Nat
1040 Rev Immunol. 2020 Aug;20(8):471–82.
1041 23. Lambotte O, Pollara J, Boufassa F, Moog C, Venet A, Haynes BF, et al. High antibody-
1042 dependent cellular cytotoxicity responses are correlated with strong CD8 T cell viral
1043 suppressive activity but not with B57 status in HIV-1 elite controllers. PloS One.
1044 2013;8(9):e74855.
1045 24. Madhavi V, Wines BD, Amin J, Emery S, ENCORE1 Study Group, Lopez E, et al. HIV-1
1046 Env- and Vpu-Specific Antibody-Dependent Cellular Cytotoxicity Responses Associated
1047 with Elite Control of HIV. J Virol. 2017 Sep 15;91(18):e00700-17.
1048 25. Rerks-Ngarm S, Pitisuttithum P, Nitayaphan S, Kaewkungwal J, Chiu J, Paris R, et al.
1049 Vaccination with ALVAC and AIDSVAX to prevent HIV-1 infection in Thailand. N Engl J
1050 Med. 2009 Dec 3;361(23):2209–20.
1051 26. Haynes BF, Gilbert PB, McElrath MJ, Zolla-Pazner S, Tomaras GD, Alam SM, et al.
1052 Immune-correlates analysis of an HIV-1 vaccine efficacy trial. N Engl J Med. 2012 Apr
1053 5;366(14):1275–86.
1054 27. Tomescu C, Tebas P, Montaner LJ. IFN-α augments natural killer-mediated antibody-
1055 dependent cellular cytotoxicity of HIV-1-infected autologous CD4+ T cells regardless of
1056 major histocompatibility complex class 1 downregulation. AIDS Lond Engl. 2017 Mar
1057 13;31(5):613–22.
1058 28. Tomescu C, Chehimi J, Maino VC, Montaner LJ. NK cell lysis of HIV-1-infected
1059 autologous CD4 primary T cells: requirement for IFN-mediated NK activation by
1060 plasmacytoid dendritic cells. J Immunol Baltim Md 1950. 2007 Aug 15;179(4):2097–104.
1061 29. Azzoni L, Foulkes AS, Papasavvas E, Mexas AM, Lynn KM, Mounzer K, et al. Pegylated
1062 Interferon alfa-2a monotherapy results in suppression of HIV type 1 replication and
1063 decreased cell-associated HIV DNA integration. J Infect Dis. 2013 Jan 15;207(2):213–
1064 22.
1065 30. Papasavvas E, Azzoni L, Pagliuzza A, Abdel-Mohsen M, Ross BN, Fair M, et al. Safety,
1066 Immune, and Antiviral Effects of Pegylated Interferon Alpha 2b Administration in
1067 Antiretroviral Therapy-Suppressed Individuals: Results of Pilot Clinical Trial. AIDS Res
1068 Hum Retroviruses. 2021 Jun;37(6):433–43.
1069 31. Hua S, Vigano S, Tse S, Zhengyu O, Harrington S, Negron J, et al. Pegylated Interferon-
1070 α-Induced Natural Killer Cell Activation Is Associated With Human Immunodeficiency

1071 Virus-1 DNA Decline in Antiretroviral Therapy-Treated HIV-1/Hepatitis C Virus-
1072 Coinfected Patients. Clin Infect Dis Off Publ Infect Dis Soc Am. 2018 Jun 1;66(12):1910–
1073 7.
1074 32. Boué F, Reynes J, Rouzioux C, Emilie D, Souala F, Tubiana R, et al. Alpha interferon
1075 administration during structured interruptions of combination antiretroviral therapy in
1076 patients with chronic HIV-1 infection: INTERVAC ANRS 105 trial. AIDS Lond Engl. 2011
1077 Jan 2;25(1):115–8.
1078 33. Papasavvas E, Azzoni L, Kossenkov AV, Dawany N, Morales KH, Fair M, et al. NK
1079 Response Correlates with HIV Decrease in Pegylated IFN-α2a-Treated Antiretroviral
1080 Therapy-Suppressed Subjects. J Immunol Baltim Md 1950. 2019 Aug 1;203(3):705–17.
1081 34. Jiao Y mei, Weng W jia, Gao Q sheng, Zhu W jun, Cai W ping, Li L hua, et al. Hepatitis
1082 C therapy with interferon-α and ribavirin reduces the CD4 cell count and the total, 2LTR
1083 circular and integrated HIV-1 DNA in HIV/HCV co-infected patients. Antiviral Res. 2015
1084 Jun;118:118–22.
1085 35. Hurst J, Hoffmann M, Pace M, Williams JP, Thornhill J, Hamlyn E, et al. Immunological
1086 biomarkers predict HIV-1 viral rebound after treatment interruption. Nat Commun. 2015
1087 Dec;6(1):8495.
1088 36. Archin NM, Liberty AL, Kashuba AD, Choudhary SK, Kuruc JD, Crooks AM, et al.
1089 Administration of vorinostat disrupts HIV-1 latency in patients on antiretroviral therapy.
1090 Nature. 2012 Jul 25;487(7408):482–5.
1091 37. Rasmussen TA, Tolstrup M, Brinkmann CR, Olesen R, Erikstrup C, Solomon A, et al.
1092 Panobinostat, a histone deacetylase inhibitor, for latent-virus reactivation in HIV-infected
1093 patients on suppressive antiretroviral therapy: a phase 1/2, single group, clinical trial.
1094 Lancet HIV. 2014 Oct;1(1):e13-21.
1095 38. Rasmussen TA, Søgaard OS, Brinkmann C, Wightman F, Lewin SR, Melchjorsen J, et
1096 al. Comparison of HDAC inhibitors in clinical development: Effect on HIV production in
1097 latently infected cells and T-cell activation. Hum Vaccines Immunother. 2013 May
1098 14;9(5):993–1001.
1099 39. Mahnke YD, Brodie TM, Sallusto F, Roederer M, Lugli E. The who's who of T-cell
1100 differentiation: Human memory T-cell subsets: HIGHLIGHTS. Eur J Immunol. 2013
1101 Nov;43(11):2797–809.
1102 40. Cano-Gamez E, Soskic B, Roumeliotis TI, So E, Smyth DJ, Baldrighi M, et al. Single-cell
1103 transcriptomics identifies an effectorness gradient shaping the response of CD4+ T cells
1104 to cytokines. Nat Commun. 2020 Dec;11(1):1801.
1105 41. Szabo PA, Levitin HM, Miron M, Snyder ME, Senda T, Yuan J, et al. Single-cell
1106 transcriptomics of human T cells reveals tissue and activation signatures in health and
1107 disease. Nat Commun. 2019 Dec;10(1):4706.
1108 42. Breton G, Chomont N, Takata H, Fromentin R, Ahlers J, Filali-Mouhim A, et al.
1109 Programmed Death-1 Is a Marker for Abnormal Distribution of Naive/Memory T Cell
1110 Subsets in HIV-1 Infection. J Immunol. 2013 Sep 1;191(5):2194–204.
1111 43. Wang S, Zhang Q, Hui H, Agrawal K, Karris MAY, Rana TM. An atlas of immune cell
1112 exhaustion in HIV-infected individuals revealed by single-cell transcriptomics. Emerg
1113 Microbes Infect. 2020 Jan 1;9(1):2333–47.
1114 44. Brinkmann CR, Højen JF, Rasmussen TA, Kjær AS, Olesen R, Denton PW, et al.
1115 Treatment of HIV-Infected Individuals with the Histone Deacetylase Inhibitor
1116 Panobinostat Results in Increased Numbers of Regulatory T Cells and Limits *Ex Vivo*
1117 Lipopolysaccharide-Induced Inflammatory Responses. Fernandez-Sesma A, editor.
1118 mSphere [Internet]. 2018 Feb 28 [cited 2021 Oct 20];3(1). Available from:
1119 https://journals.asm.org/doi/10.1128/mSphere.00616-17
1120 45. Kazmierski J, Elsner C, Döhner K, Xu S, Ducroux A, Pott F, et al. A Baseline Cellular
1121 Antiviral State Is Maintained by cGAS and Its Most Frequent Naturally Occurring Variant
1122 rs610913. J Immunol Baltim Md 1950. 2022 Jul 18;ji2100685.
1123 46. Perez VL, Rowe T, Justement JS, Butera ST, June CH, Folks TM. An HIV-1-infected T
1124 cell clone defective in IL-2 production and Ca2+ mobilization after CD3 stimulation. J
1125 Immunol Baltim Md 1950. 1991 Nov 1;147(9):3145–8.

1126 47. Symons J, Chopra A, Malatinkova E, De Spiegelaere W, Leary S, Cooper D, et al. HIV
1127 integration sites in latently infected cell lines: evidence of ongoing replication.
1128 Retrovirology. 2017 Dec;14(1):2.
1129 48. Jamaluddin MS, Hu PW, Jan Y, Siwak EB, Rice AP. Short Communication: The Broad-
1130 Spectrum Histone Deacetylase Inhibitors Vorinostat and Panobinostat Activate Latent
1131 HIV in CD4+ T Cells In Part Through Phosphorylation of the T-Loop of the CDK9 Subunit
1132 of P-TEFb. AIDS Res Hum Retroviruses. 2016 Feb 1;32(2):169–73.
1133 49. Harper MS, Guo K, Gibbert K, Lee EJ, Dillon SM, Barrett BS, et al. Interferon-α
1134 Subtypes in an Ex Vivo Model of Acute HIV-1 Infection: Expression, Potency and
1135 Effector Mechanisms. PLoS Pathog. 2015;11(11):e1005254.
1136 50. Lavender KJ, Gibbert K, Peterson KE, Van Dis E, Francois S, Woods T, et al. Interferon
1137 Alpha Subtype-Specific Suppression of HIV-1 Infection In Vivo. J Virol. 2016 Jul
1138 1;90(13):6001–13.
1139 51. Karakoese Z, Schwerdtfeger M, Karsten CB, Esser S, Dittmer U, Sutter K. Distinct Type
1140 I Interferon Subtypes Differentially Stimulate T Cell Responses in HIV-1-Infected
1141 Individuals. Front Immunol. 2022;13:936918.
1142 52. Guo K, Shen G, Kibbie J, Gonzalez T, Dillon SM, Smith HA, et al. Qualitative Differences
1143 Between the IFNα subtypes and IFNβ Influence Chronic Mucosal HIV-1 Pathogenesis.
1144 PLoS Pathog. 2020 Oct;16(10):e1008986.
1145 53. Tsai P, Wu G, Baker CE, Thayer WO, Spagnuolo RA, Sanchez R, et al. In vivo analysis
1146 of the effect of panobinostat on cell-associated HIV RNA and DNA levels and latent HIV
1147 infection. Retrovirology. 2016 Dec;13(1):36.
1148 54. Bartholomeeusen K, Fujinaga K, Xiang Y, Peterlin BM. Histone Deacetylase Inhibitors
1149 (HDACis) That Release the Positive Transcription Elongation Factor b (P-TEFb) from Its
1150 Inhibitory Complex Also Activate HIV Transcription. J Biol Chem. 2013 May
1151 17;288(20):14400–7.
1152 55. Khoury G, Mota TM, Li S, Tumpach C, Lee MY, Jacobson J, et al. HIV latency reversing
1153 agents act through Tat post translational modifications. Retrovirology. 2018 May
1154 11;15(1):36.
1155 56. Kwaa AKR, Talana CAG, Blankson JN. Interferon Alpha Enhances NK Cell Function and
1156 the Suppressive Capacity of HIV-Specific CD8+ T Cells. J Virol. 2019 Jan
1157 17;93(3):e01541-18.
1158 57. Edens RE, Dagtas S, Gilbert KM. Histone deacetylase inhibitors induce antigen specific
1159 anergy in lymphocytes: a comparative study. Int Immunopharmacol. 2006
1160 Nov;6(11):1673–81.
1161 58. Pace M, Williams J, Kurioka A, Gerry AB, Jakobsen B, Klenerman P, et al. Histone
1162 Deacetylase Inhibitors Enhance CD4 T Cell Susceptibility to NK Cell Killing but Reduce
1163 NK Cell Function. Swanstrom R, editor. PLOS Pathog. 2016 Aug 16;12(8):e1005782.
1164 59. Triplett TA, Holay N, Kottapalli S, VanDenBerg C, Capasso A. Elucidating the Role of
1165 HDACs in T Cell Biology and Comparing Distinct HDAC Inhibitors in Augmenting
1166 Responses to Cancer Immunotherapy. J Immunol. 2020 Mai;204(1 Supplement):165.23.
1167 60. Jones RB, O'Connor R, Mueller S, Foley M, Szeto GL, Karel D, et al. Histone
1168 Deacetylase Inhibitors Impair the Elimination of HIV-Infected Cells by Cytotoxic T-
1169 Lymphocytes. Silvestri G, editor. PLoS Pathog. 2014 Aug 14;10(8):e1004287.
1170 61. Boucau J, Das J, Joshi N, Le Gall S. Latency reversal agents modulate HIV antigen
1171 processing and presentation to CD8 T cells. PLoS Pathog. 2020 Mar;16(3):e1008442.
1172 62. Nusinzon I, Horvath CM. Positive and negative regulation of the innate antiviral response
1173 and beta interferon gene expression by deacetylation. Mol Cell Biol. 2006
1174 Apr;26(8):3106–13.
1175 63. von Schwedler UK, Stray KM, Garrus JE, Sundquist WI. Functional Surfaces of the
1176 Human Immunodeficiency Virus Type 1 Capsid Protein. J Virol. 2003 May;77(9):5439–
1177 50.
1178 64. Anokhin B, Spearman P. Viral and Host Factors Regulating HIV-1 Envelope Protein
1179 Trafficking and Particle Incorporation. Viruses. 2022 Aug;14(8):1729.
1180 65. von Bredow B, Arias JF, Heyer LN, Gardner MR, Farzan M, Rakasz EG, et al. Envelope

1181 Glycoprotein Internalization Protects Human and Simian Immunodeficiency Virus-
1182 Infected Cells from Antibody-Dependent Cell-Mediated Cytotoxicity. J Virol. 2015
1183 Oct;89(20):10648–55.
1184 66. Veillette M, Coutu M, Richard J, Batraville LA, Dagher O, Bernard N, et al. The HIV-1
1185 gp120 CD4-bound conformation is preferentially targeted by antibody-dependent cellular
1186 cytotoxicity-mediating antibodies in sera from HIV-1-infected individuals. J Virol. 2015
1187 Jan;89(1):545–51.
1188 67. Veillette M, Désormeaux A, Medjahed H, Gharsallah NE, Coutu M, Baalwa J, et al.
1189 Interaction with cellular CD4 exposes HIV-1 envelope epitopes targeted by antibody-
1190 dependent cell-mediated cytotoxicity. J Virol. 2014 Mar;88(5):2633–44.
1191 68. Xu HC, Grusdat M, Pandyra AA, Polz R, Huang J, Sharma P, et al. Type I interferon
1192 protects antiviral CD8+ T cells from NK cell cytotoxicity. Immunity. 2014 Jun
1193 19;40(6):949–60.
1194 69. Crouse J, Bedenikovic G, Wiesel M, Ibberson M, Xenarios I, Von Laer D, et al. Type I
1195 interferons protect T cells against NK cell attack mediated by the activating receptor
1196 NCR1. Immunity. 2014 Jun 19;40(6):961–73.
1197 70. Pham TN, Lukhele S, Hajjar F, Routy JP, Cohen ÉA. HIV Nef and Vpu protect HIV-
1198 infected CD4+ T cells from antibody-mediated cell lysis through down-modulation of CD4
1199 and BST2. Retrovirology. 2014 Feb 6;11(1):15.
1200 71. Azzoni L, Foulkes AS, Papasavvas E, Mexas AM, Lynn KM, Mounzer K, et al. Pegylated
1201 Interferon Alfa-2a Monotherapy Results in Suppression of HIV Type 1 Replication and
1202 Decreased Cell-Associated HIV DNA Integration. J Infect Dis. 2013 Jan 15;207(2):213–
1203 22.
1204 72. Asmuth DM, Murphy RL, Rosenkranz SL, Lertora JJL, Kottilil S, Cramer Y, et al. Safety,
1205 tolerability, and mechanisms of antiretroviral activity of pegylated interferon Alfa-2a in
1206 HIV-1-monoinfected participants: a phase II clinical trial. J Infect Dis. 2010 Jun
1207 1;201(11):1686–96.
1208 73. Ogbomo H, Michaelis M, Kreuter J, Doerr HW, Cinatl J. Histone deacetylase inhibitors
1209 suppress natural killer cell cytolytic activity. FEBS Lett. 2007 Apr 3;581(7):1317–22.
1210 74. Gruell H, Gunst JD, Cohen YZ, Pahus MH, Malin JJ, Platten M, et al. Effect of 3BNC117
1211 and romidepsin on the HIV-1 reservoir in people taking suppressive antiretroviral therapy
1212 (ROADMAP): a randomised, open-label, phase 2A trial. Lancet Microbe. 2022
1213 Mar;3(3):e203–14.
1214 75. Gay CL, James KS, Tuyishime M, Falcinelli SD, Joseph SB, Moeser MJ, et al. Stable
1215 Latent HIV Infection and Low-level Viremia Despite Treatment With the Broadly
1216 Neutralizing Antibody VRC07-523LS and the Latency Reversal Agent Vorinostat. J Infect
1217 Dis. 2022 Mar 2;225(5):856–61.
1218 76. Leth S, Schleimann MH, Nissen SK, Højen JF, Olesen R, Graversen ME, et al.
1219 Combined effect of Vacc-4x, recombinant human granulocyte macrophage colony-
1220 stimulating factor vaccination, and romidepsin on the HIV-1 reservoir (REDUC): a single-
1221 arm, phase 1B/2A trial. Lancet HIV. 2016 Oct;3(10):e463-472.
1222 77. Machnowska P, Meixenberger K, Schmidt D, Jessen H, Hillenbrand H, Gunsenheimer-
1223 Bartmeyer B, et al. Prevalence and persistence of transmitted drug resistance mutations
1224 in the German HIV-1 Seroconverter Study Cohort. PloS One. 2019;14(1):e0209605.
1225 78. Butler A, Hoffman P, Smibert P, Papalexi E, Satija R. Integrating single-cell
1226 transcriptomic data across different conditions, technologies, and species. Nat
1227 Biotechnol. 2018 Jun;36(5):411–20.
1228 79. MacLeod MKL, Clambey ET, Kappler JW, Marrack P. CD4 memory T cells: What are
1229 they and what can they do? Semin Immunol. 2009 Apr 1;21(2):53–61.
1230 80. Chomont N, El-Far M, Ancuta P, Trautmann L, Procopio FA, Yassine-Diab B, et al. HIV
1231 reservoir size and persistence are driven by T cell survival and homeostatic proliferation.
1232 Nat Med. 2009 Aug;15(8):893–900.
1233 81. Pušnik J, Eller MA, Tassaneetrithep B, Schultz BT, Eller LA, Nitayaphan S, et al.
1234 Expansion of Stem Cell-Like CD4+ Memory T Cells during Acute HIV-1 Infection Is
1235 Linked to Rapid Disease Progression. J Virol. 2019 Jun 28;93(14):e00377-19.

1236 82. Kononchik J, Ireland J, Zou Z, Segura J, Holzapfel G, Chastain A, et al. HIV-1 targets L-
1237 selectin for adhesion and induces its shedding for viral release. Nat Commun. 2018 Jul
1238 19;9(1):2825.
1239 83. Golubovskaya V, Wu L. Different Subsets of T Cells, Memory, Effector Functions, and
1240 CAR-T Immunotherapy. Cancers. 2016 Mar 15;8(3):36.
1241 84. Jain N, Nguyen H, Chambers C, Kang J. Dual function of CTLA-4 in regulatory T cells
1242 and conventional T cells to prevent multiorgan autoimmunity. Proc Natl Acad Sci. 2010
1243 Jan 26;107(4):1524–8.
1244 85. Jiang Y, Li Y, Zhu B. T-cell exhaustion in the tumor microenvironment. Cell Death Dis.
1245 2015 Jun;6(6):e1792–e1792.
1246 86. Ramírez F, Ryan DP, Grüning B, Bhardwaj V, Kilpert F, Richter AS, et al. deepTools2: a
1247 next generation web server for deep-sequencing data analysis. Nucleic Acids Res. 2016
1248 Jul 8;44(W1):W160-165.
1249 87. Metsalu T, Vilo J. ClustVis: a web tool for visualizing clustering of multivariate data using
1250 Principal Component Analysis and heatmap. Nucleic Acids Res. 2015 Jul
1251 1;43(W1):W566-570.
1252 88. Wang J, Duncan D, Shi Z, Zhang B. WEB-based GEne SeT AnaLysis Toolkit
1253 (WebGestalt): update 2013. Nucleic Acids Res. 2013 Jul;41(Web Server issue):W77-83.
1254 89. Zhang B, Kirov S, Snoddy J. WebGestalt: an integrated system for exploring gene sets
1255 in various biological contexts. Nucleic Acids Res. 2005 Jul 1;33(Web Server
1256 issue):W741–8.
1257 90. Mi H, Thomas P. PANTHER Pathway: an ontology-based pathway database coupled
1258 with data analysis tools. Methods Mol Biol Clifton NJ. 2009;563:123–40.
1259 91. Garcia-Alonso L, Holland CH, Ibrahim MM, Turei D, Saez-Rodriguez J. Benchmark and
1260 integration of resources for the estimation of human transcription factor activities.
1261 Genome Res. 2019 Aug;29(8):1363–75.
1262 92. Holland CH, Tanevski J, Perales-Patón J, Gleixner J, Kumar MP, Mereu E, et al.
1263 Robustness and applicability of transcription factor and pathway analysis tools on single-
1264 cell RNA-seq data. Genome Biol. 2020 Feb 12;21(1):36.
1265 93. Jassal B, Matthews L, Viteri G, Gong C, Lorente P, Fabregat A, et al. The reactome
1266 pathway knowledgebase. Nucleic Acids Res. 2020 Jan 8;48(D1):D498–503.
1267 94. Liberzon A, Subramanian A, Pinchback R, Thorvaldsdóttir H, Tamayo P, Mesirov JP.
1268 Molecular signatures database (MSigDB) 3.0. Bioinforma Oxf Engl. 2011 Jun
1269 15;27(12):1739–40.
1270 95. Laue M. Electron microscopy of viruses. Methods Cell Biol. 2010;96:1–20.
1271 96. Richard J, Veillette M, Batraville LA, Coutu M, Chapleau JP, Bonsignori M, et al. Flow
1272 cytometry-based assay to study HIV-1 gp120 specific antibody-dependent cellular
1273 cytotoxicity responses. J Virol Methods. 2014 Nov;208:107–14.
1274 97. Alter G, Malenfant JM, Altfeld M. CD107a as a functional marker for the identification of
1275 natural killer cell activity. J Immunol Methods. 2004 Nov;294(1–2):15–22.
1276